GEOLOGICA CARPATHICA, AUGUST 2023, 74, 4, 325–346 https://doi.org/10.31577/GeolCarp.2023.17

Systematics of clinopyroxene phenocrysts, megacrysts, and cumulates in Tertiary basalts of southern Slovakia with implications in the structure of lithospheric mantle

VRATISLAV HURAI[1,✉], MONIKA HURAIOVÁ[2], ONDREJ NEMEC[2], PATRIK KONEČNÝ[3] and LUCA REATO[2]

[1]Earth Science Institute of the Slovak Academy of Sciences, Bratislava, Slovakia; ✉vratislav.hurai@savba.sk
[2]Faculty of Sciences, Department of Mineralogy, Petrology and Raw Materials, Comenius University, Bratislava, Slovakia
[3]State Geological Institute of Dionýz Štúr, Bratislava, Slovakia

(Manuscript received April 25, 2023; accepted in revised form August 15, 2023; Associate Editor: Milan Kohút)

Abstract: Tertiary alkali basalts in the South-Slovakian Basin contain homogeneous clinopyroxene megacrysts, composite phenocrysts with chemically and optically homogeneous olive-green cores overgrown by oscillatory zoned rims, and fragments of clinopyroxene-rich igneous cumulates. Discrimination based on Ca, Na, Ti and Cr concentrations defined clinopyroxenes with alkalic, tholeiitic and transitional affinities. Single-pyroxene thermobarometry revealed that the incipient clinopyroxene crystallization occurred at 1300–1350 °C and 2.0–2.2 GPa, thus identifying the zone of mantle melting in a depth of >70 km. The highest frequency of pressure data from clinopyroxene-rich mafic cumulates, betwen 0.7 and 1.2 GPa, indicate stagnant basaltic reservoirs located beneath the Moho discontinuity, 30–43 km deep. Late fractionation products of alkali basalt derivatives may have occurred as laccoliths and dykes in the lower crust. Thermodynamic modelling of mineral assemblages of cumulate xenoliths revealed that parental melts for both alkalic and tholeiitic affinities were silica-undersaturated (46–46.5 wt. % SiO_2) and moderately alkalic (index of alkalinity 2.0–3.8, Mg# ~50) basalt to basanite, with pre-eruptive water contents between 1 and 2 wt. %. Amphibole–biotite–titanite–ilmenite–plagioclase cumulates recorded the advanced stage of fractionation of more calcic basalt at 900–920 °C and 0.65 GPa. Deep-seated basalt reservoirs have been less alkalic than erupted lavas, the latter showing a Mg depletion and an increasing aluminium saturation index diagnostic of the extensive crystal separation on the way to the surface. Olive-green megacrysts and cores of zoned phenocrysts originated at lower temperatures and higher pressures than their autocrystic rims. The megacrystic assemblage of Fe-diopside–Al-augite, Mg-calcite, apatite, ulvöspinel, and disintegrated amphibole crystallized from evolved, relatively cold (~950–1100 °C), Fe-rich carbonatite–alkalic silicate melt within the depth interval of 26–53 km, corresponding to a lithostatic pressure of 0.7–1.5 GPa. The silicate–carbonate–phosphate melt fraction probably originated in the subducting slab of oceanic crust.

Keywords: clinopyroxene megacryst, clinopyroxene phenocryst, clinopyroxene cumulate, basalt fractionation, basalt underplating, ALCAPA

Introduction

Intra-plate basalts in the South-Slovakian Basin (SSB) in the Novohrad–Gemer (Nógrád–Gömör) region contain several types of clinopyroxene crystals: (1) zoned autocrysts (=phenocrysts) nucleating from the ascending basaltic magma; (2) chemically and optically homogeneous antecrysts (=megacrysts) cogenetic with the intra-plate magmatism, but out of equilibrium with the basalt host; (3) combined crystals composed of antecrystic cores surrounded by autocrystic rims; (4) xenocrysts of an unknown origin unrelated with basalt volcanism. Apart from the crystals, fragments of clinopyroxene-bearing mafic gravitational cumulates from bottom parts of magmatic reservoirs (gabbro, pyroxenite, hornblendite) and felsic flotation cumulates (syenite) from their upper parts have also been described.

Here we summarize electron probe microanalytical data (EPMA) on various types of magmatic clinopyroxenes in intra-plate basalts and volcanoclastic deposits of the SSB with the aim of defining their diagnostic compositional characteristics and elucidating *P–T* parameters of parental magmas. Thermobarometric data are employed for the localization of deep magmatic reservoirs and the reconstruction of lithospheric structure. Thermodynamic modelling helps in the determination of pre-eruptive water contents in parental basalts and discrimination of possible melt parents of igneous cumulate xenoliths and megacrysts. Finally, we define pristine basalt types unaffected by the fractionation and put forward a genetic model of alkali basalts erupted as monogenetic volcanoes in the study area.

Geological setting

Based on the regional morphological and geographical subdivision (Vass et al. 1988a), the South-Slovakian Basin (SSB) can be subdivided into the Cerová Upland surrounded by the Lučenec Basin in the west and the Rimava Basin in

the northeast, which all are the northernmost promontories of the intra-Carpathian back-arc basin (Pannonian Basin) developed as a response to the Alpine-Carpathian orogenic belt formation (Fig. 1). The SSB is located in the Alpine–Carpathian–Pannonian (ALCAPA) tectonic mega-unit separated from the Tisza–Dacia mega-unit in the south during the Late Oligocene–Early Miocene extrusion and escape from the Alpine collision zone (Kázmér & Kovács 1985; Csontos 1995). Marine sedimentation in the Pannonian Basin started approximately 19 Ma ago (Royden et al. 1983) during the Early Miocene extension driven by the subduction and roll-back of the oceanic crust in eastern segments of the orogenic belt (Nemcok et al. 1998; Konečný et al. 2002).

The SSB is filled with Oligocene–Upper Miocene (Kiscellian Číž Formation and Eggerian Lučenec Formation) and Lower Miocene (Eggenburgian Fiľakovo and Bukovinka Formations) marine sediments discordantly overlain by lacustrine sediments of Upper Miocene (Pontian) Poltár Formation in the Lučenec Basin and fluvial sediments (gravels and sandstones) of Upper Pliocene Belina beds preserved at the base of basaltic lava flows in the Cerová Upland. The commonly accepted Romanian age of Belina beds is, however, in conflict with an Early Pliocene (Dacian) age of the overlying lava flow of Belinský vrch, S–SW from Čamovce village (Huraiová et al. 2017; Fig. 1).

The Pre-Cenozoic basement cropping out in northern margins of the SSB corresponds to Veporicum, Gemericum, Turnaicum, Silicicum and Melaticum tectonic units of Inner Western Carpathians, continually dipping southwards beneath the SSB sedimentary infilling (e.g., Vass et al. 1988b; Dzúrik

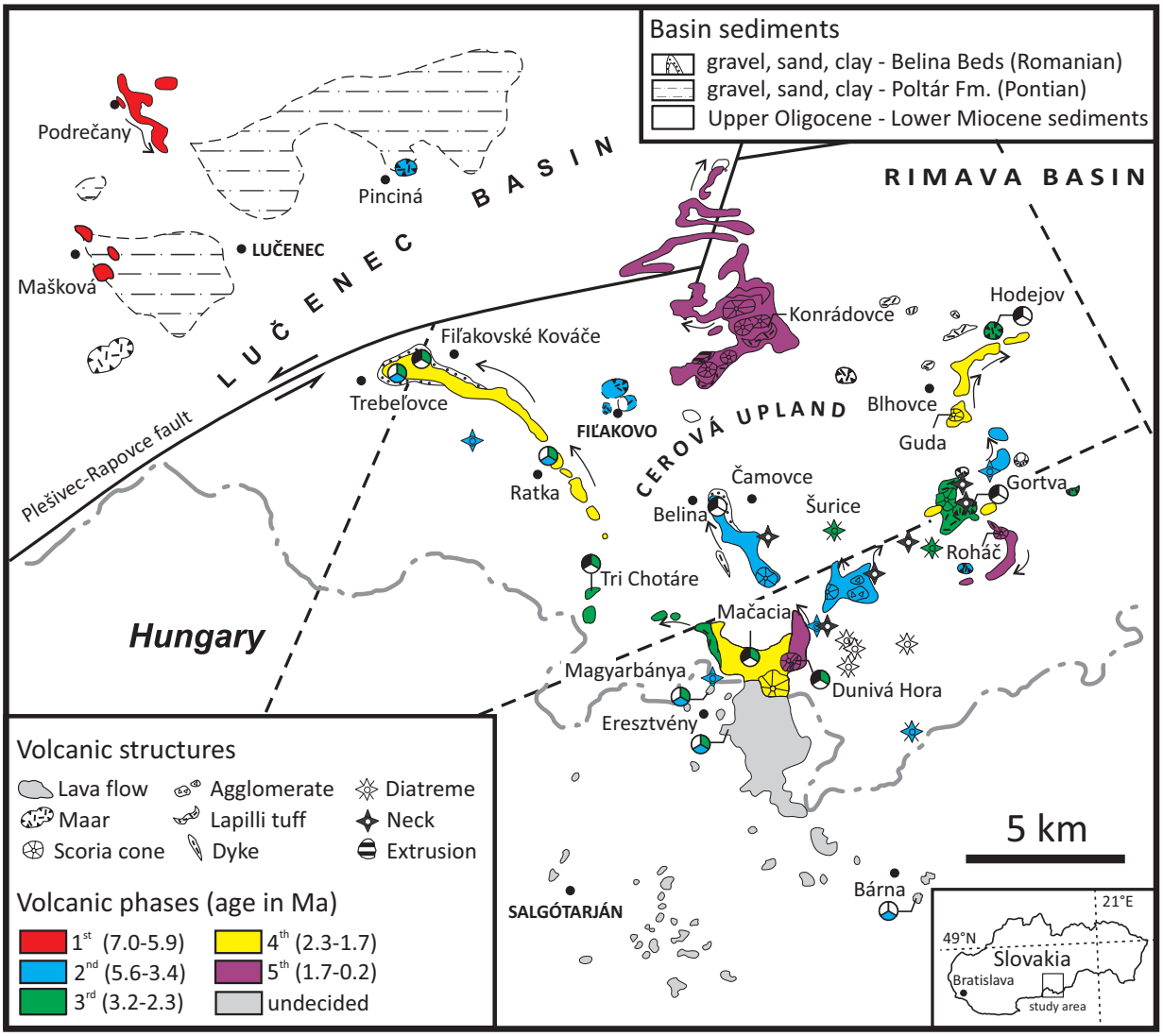

Fig. 1. Schematic geological map of the South-Slovakian Basin (SSB) modified after Konečný et al. (2004), with major tectonic lines (dashed) redrawn from Vass et al. (2007) and supplemented by K–Ar basalt (Konečný et al. 2004), U–Pb zircon, (U–Th/He) zircon and apatite, and U–Th monazite geochronological data (Hurai et al. 2010, 2013; Huraiová et al. 2017; Paquette et al. 2019). Pie diagrams indicate occurrences of mantle xenoliths (green sector), igneous cumulate xenoliths (black sector) and/or olive-green clinopyroxene megacrysts (blue sector) in localities studied. The older Podrečany Formation comprises lava flows and maars northwest of the Plešivec–Rapovce transform fault.

et al. 2007). Tectonic affiliation of the basement south from the SW–NE-striking Rapovce–Plešivec transform fault (Fig. 1) is ambiguous and only based on a relatively shallow (~2 km) borehole near Blhovce (FV-1) and the composition of xenolith cargo brought to the surface by basalts. Low-grade metamorphic rocks (greenschist, phyllite) intercepted by the FV-1 borehole are correlated with either the Gemericum superunit of southern Slovakia (Snopková & Bajaník 1979; Vass et al. 2007) or the Aggtelek–Rudabánya unit of northern Hungary (Dank & Fülöp 1990). Gneiss and amphibolite xenoliths in Miocene andesite laccoliths of the Karanč–Šiatoroš volcanic complex south of Fiľakovo town have been tentatively correlated with the Veporicum superunit (Hovorka & Lukáčik 1972) or the Meliaticum unit (Plašienka et al. 1997).

About 30 km thick crust in the study region (Janik et al. 2011; Horváth et al. 2015; Klébesz et al. 2015) is underlain by the lithospheric mantle. The mantle–asthenosphere boundary (LAB) is provisionally located in the depth of ~70 km (Tašárová et al. 2009; Bielik et al. 2010; Klébesz et al. 2015).

The back-arc sedimentation in the Pannonian Basin was accompanied by several episodes of syn- and post-collisional magmatism, of which the Late Miocene–Pleistocene Na-alkaline continental basalt volcanism is dominant in the study area (Fig. 1). Middle-Miocene andesite laccoliths (Bouloton & Paquette 2014) occur south of Fiľakovo town. Compositional types of basalts comprise abundant basanite/tephrite, less frequent trachybasalt, phonotephrite and basaltic trachyandesite, and rare basalt (Fig. 2). The index of alkalinity, $IA = Na_2O + K_2O - 0.37 \times (SiO_2 - 39)$, expressed as a deviation from the division line defined by Macdonald & Katsura (1964), ranges between 1.8 and 5.0, showing alkalic character of all basalt types (Electronic Supplementary Material, Supplementary Table S1).

Surprising feature of the basalt volcanism is that it postdates the extension ceased by the Late Miocene in the Pannonian Basin (Horváth et al. 2015). Consequently, a variety of mechanisms have been proposed to explain the basalt melt generation. Decompression melting by asthenospheric upwelling (Embey-Isztin & Dobosi 1995; Konečný et al. 2002) is the most popular model. Finger-like asthenospheric plumes, lithospheric edge-related mantle flow, compression of hydrated asthenospheric dome, and plate tectonic processes have also been proposed as possible alternatives (Wilson & Downes 1991; Embey-Isztin et al. 1993; Seghedi et al. 2004, 2011; Harangi et al. 2015; Kovács et al. 2020).

The SSB basalts erupted as monogenetic volcanoes (Lexa et al. 2010) within the time interval from ~7 Ma to ~200 ka (Pécskay et al. 2006; Vass et al. 2007) during a total of six volcanic phases defined according to K/Ar radiometric dating of lava flows, necks and dykes (Konečný V. et al. 1995, 1999; Vass et al. 2007). The initial Late Miocene volcanic phase recently known as the Podrečany Basalt Formation (Balogh et al. 1981; Vass & Kraus 1985) was identified in the Lučenec Basin, where a basanitic lava flow near Podrečany village (Fig. 1) returned K/Ar whole-rock and isochron ages corresponding to 6.4±0.3 and 6.2±0.5 Ma, respectively. Maars near Jelšovec and Pinciná villages were also affiliated with the first volcanic phase according to their position below fluvial–lacustrine sediments of the Poltár Formation, whose Late Miocene (Pontian) age was inferred from sporomorphs (Planderová 1986). However, the Pinciná maar age was later redefined to 5.4±0.1 Ma using U–Th/He data on zircons (Hurai et al. 2013), thus indirectly constraining the Early Pliocene age limit for the overlying Poltár Formation.

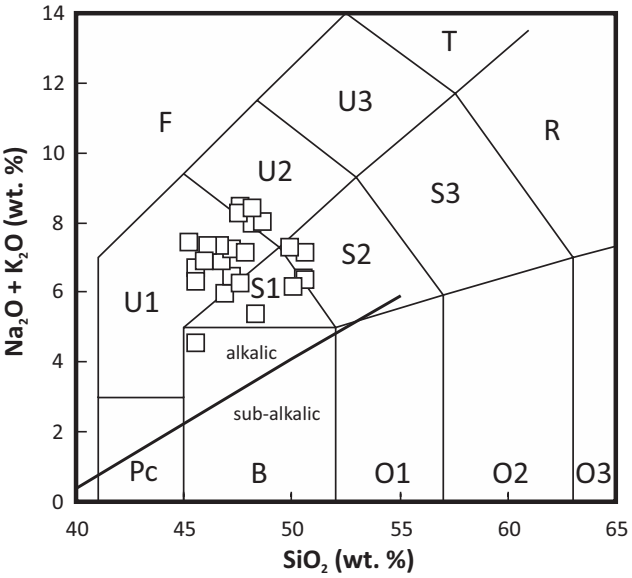

Fig. 2. Total alkalis versus SiO_2 (TAS) classification diagram (Le Maitre et al. 2002) for SSB basalts (open squares, n = 23). Abbreviations: F – foidite, Pc – picrite, B – basalt, O1 – basaltic andesite, O2 – andesite, O3 – dacite, S1 – trachybasalt, S2 – basaltic trachyandesite, S3 – trachyandesite, R – rhyolite, U1 – basanite/tephrite, U2 – phonotephrite, U3 – tephriphonolite, T – trachyte/trachydacite. Division line separating alkalic and sub-alkalic magmas is after Macdonald & Katsura (1964).

The Pliocene–Quaternary volcanism of the Cerová Upland is affiliated with the Cerová Basalt Formation erupted in dry land conditions (Vass & Kraus 1985). Lava flows, domes, necks and plugs have been produced by the effusive volcanism, whereas phreatic and phreato–magmatic eruptions have given rise to maar depressions, tuff rings, scoria and spatter cones (Lexa et al. 2010) later partially removed by erosion during vertical tectonic movements. The same process also exposed resistant diatremes representing maar feeder conduits. The 1.02±0.1 Ma old lava neck of the Roháč (Ragáč) scoria cone correlated with 5th volcanic phase is the youngest structure of the Cerová Upland directly dated by the K/Ar method. The Late Pleistocene 6th phase was only identified as occurrences of volcanic tuffs overlying Quaternary river terraces (Vass et al. 2007). The presumably Late Pleistocene ages of maars near Hodejov village and under Fiľakovo castle were discredited by the U–Th/He apatite, U–Pb zircon and U–Th/He zircon geochronology, which yielded ages of 2.8±0.2 and 5.4±0.7 Ma, respectively (Hurai et al. 2013).

Analytical and interpretation methods

This review is based on a total of 603 electron probe microanalyses (EPMA) of clinopyroxenes obtained in the last 20 years in laboratories of Geological Institute of D. Štúr in Bratislava under supervision of P. Konečný using a Cameca SX-100 electron probe micro-analyser (Supplementary Table S2). The device was calibrated with the following mineral and synthetic reference materials (measured lines and crystals in parentheses): albite – Na (Kα, TAP), SiO_2 – Si (Kα, TAP), orthoclase – K (Kα, LPET), Al_2O_3 – Al (Kα, TAP), MgO – Mg (Kα, TAP), wollastonite – Ca (Kα, LPET), fayalite – Fe (Kα, LLIF), rhodonite – Mn (Kα, LLIF), TiO_2 – Ti (Kα, LPET), Cr_2O_3 – Cr (Kα, LLIF). A 15 kV accelerating voltage, 20 nA beam current, and 5 µm beam diameter were used to optimise the spatial resolution, matrix correction factors, and to minimise surface damage. Sample/background counting times were as follows (s): Na, K, Mg, Ca, Si, Al, Ti (10/5), Mn, Fe, Cr (30/15). Matrix effects were resolved using the X–φ correction method (Merlet 1992). Average detection limits (±3σ) were as follows (ppm): Na – 277±16, Si – 181±5, K – 118±4, Al – 170±8, Mg – 194±8, Mn – 367±20, Ca – 128±6, Fe – 380±20, Ti – 155±5, Cr – 324±16. Standard deviations of replicate measurements (±1σ) varied between 0.02 and 0.3 wt. %. The obtained dataset was supplemented by published EPMA from green clinopyroxene megacrysts from Ratka, Magyarbánya, Eresztvény and Bárna (Dobosi & Jenner 1999).

The single-clinopyroxene thermobarometer is based on the following equilibrium (Putirka et al. 1996; Putirka 2008):

$$2SiO_2^{liq} + NaO_{1/2}^{liq} + AlO_{3/2}^{liq} = NaAlSi_2O_6^{Jd} \quad \text{(Eqn. 1)}$$

where Jd denotes the jadeite component in clinopyroxene, and quantities with superscript ^{liq} are the cation fractions of the given oxide in the liquid.

Clinopyroxene components are calculated from cation proportions using a normative procedure (Putirka et al. 2003):

$$X_{EnFs} = X_{Fe} - X_{Fe}^{3+} + X_{Mg} - X_{DiHd}$$
$$X_{DiHd} = X_{Ca} - X_{CaTi} - X_{CaTs} - X_{CrCaTs}$$
$$X_{CaTi} = X_{Al}^{IV} - X_{CaTs}$$
$$X_{CaTs} = X_{Al}^{VI} - X_{Jd}$$
$$X_{CrCaTs} = X_{Cr}/2$$
$$X_{Jd} = \mathrm{MIN}(X_{Na}, X_{Al}^{IV})$$

Ferric iron content was calculated according to Droop (1987) as

$$Fe^{3+} = 12 \times (1 - 4/\Sigma \text{ cations}).$$

Putirka (2008) derived the following thermobarometer based on the Jd–DiHd–EnFs exchange:

$$P\,(\text{kbar}) = 3205 + 0.384T - 518\ln T - 5.62X_{Mg} + 83.2X_{Na} + 68.2X_{DiHd} + 2.52\ln X_{Al}^{VI} - 51.1X_{DiHd}^2 + 34.8X_{EnFs}^2 \quad \text{(Eqn. 2)}$$

$$T\,(\text{K}) = (93100 + 544P)/[61.1 + 36.6X_{Ti} + 10.9X_{Fe} - 0.95(X_{Al} + X_{Cr} - X_{Na} - X_K) + 0.395(\ln a_{En})^2] \quad \text{(Eqn. 3)}$$

where the activity of enstatite is calculated as $a_{En} = (1 - X_{Ca} - X_{Na} - X_K) \times [1 - 0.5 \times (X_{Al} + X_{Cr} + X_{Na} + X_K)]$ (Nimis & Taylor 2000) and temperature and pressure for given composition can be calculated from Eqns. 2 and 3 by iteration. The Jd–DiHd–EnFs exchange thermobarometer reproduces the anhydrous experimental dataset to ±58 °C and ±0.31 GPa (1σ).

Thermodynamic calculations were made using the Gibbs energy minimization method performed in the 2D mode (P–T coordinates) or along estimated cooling trajectories with the help of a Perple_X computer program, version 6.9.1 (Connolly 2005, 2009; https://www.perplex.ethz.ch/perplex/ibm_and_mac_archives). Thermodynamic database hp633ver.dat and solution models for silicate melt – melts(HGPH), garnet – Gt(HGP), spinel – Sp(HGP), biotite – Bi(HGP) and clinopyroxene – Cpx(HGP) (Holland et al. 2018), plagioclase – Pl(JH) (Jennings & Holland 2015), and amphibole – cAmph(DP) (Diener et al. 2007), were employed. The O_2 saturation in the KNCMFATSHO system was controlled by the fayalite–ferrosilite+magnetite buffer.

Petrography

Phenocrysts and megacrysts

Explosive, extrusive and effusive products of basalt volcanism of the SSB contain several types of clinopyroxene crystals and crystal fragments: (1) optically and chemically homogeneous, angular fragments or rounded crystals, up to several cm in diameter (megacrysts); (2) smaller, up to 500 µm in size, oscillatory and chemically zoned autocrysts (phenocrysts); (3) combined crystals with ideal external morphology consisting of irregular, optically homogeneous megacrystic cores surrounded by rhythmically banded autocrystic margins; (4) xenocrysts scavenged from the upper mantle and the lower crust.

Dark green to black, almost opaque megacrysts with glassy lustre, up to 2 cm in diameter, occur in basaltic and basanitic lava flows in Mašková, Fiľakovské Kováče, Ratka, Bárna, Eresztvény, and Magyarbánya. Clinopyroxene megacrysts identified in the Pinciná maar are homogeneous resorbed grains, up to 500 µm in diameter, surrounded by a thin reaction rim. Angular clinopyroxene megacrystic cores are surrounded by thick oscillatory zoned, finely banded autocrystic margin in effusive basalts of Mašková (Fig. 3A–F). Similar angular cores, olive-green in transmitted light, occur in basanites from Ratka, where they grade into oscillatory zoned light-green and light-brown margins with perfect outer crystal morphology (Fig. 3G–H). The olive-green megacrysts also occur in the lava flow as solitary anhedral fragments, up to 2 cm in size, surrounded by very thin epitaxial layer, less than 20 µm thick, of brown clinopyroxene.

Apart from clinopyroxene, the megacrystic assemblage of Ratka and Mašková basalts also involves anhedral opaque grains of ulvöspinel–magnetite series, partially resorbed fluorapatite crystals (Fig. 4A), and semi-opaque pseudomorphs composed of finely-grained nepheline, ulvöspinel, forsterite, $An_{60–66}$ plagioclase, Al–Ti-rich augite, and rhönite (Fig. 4B, C).

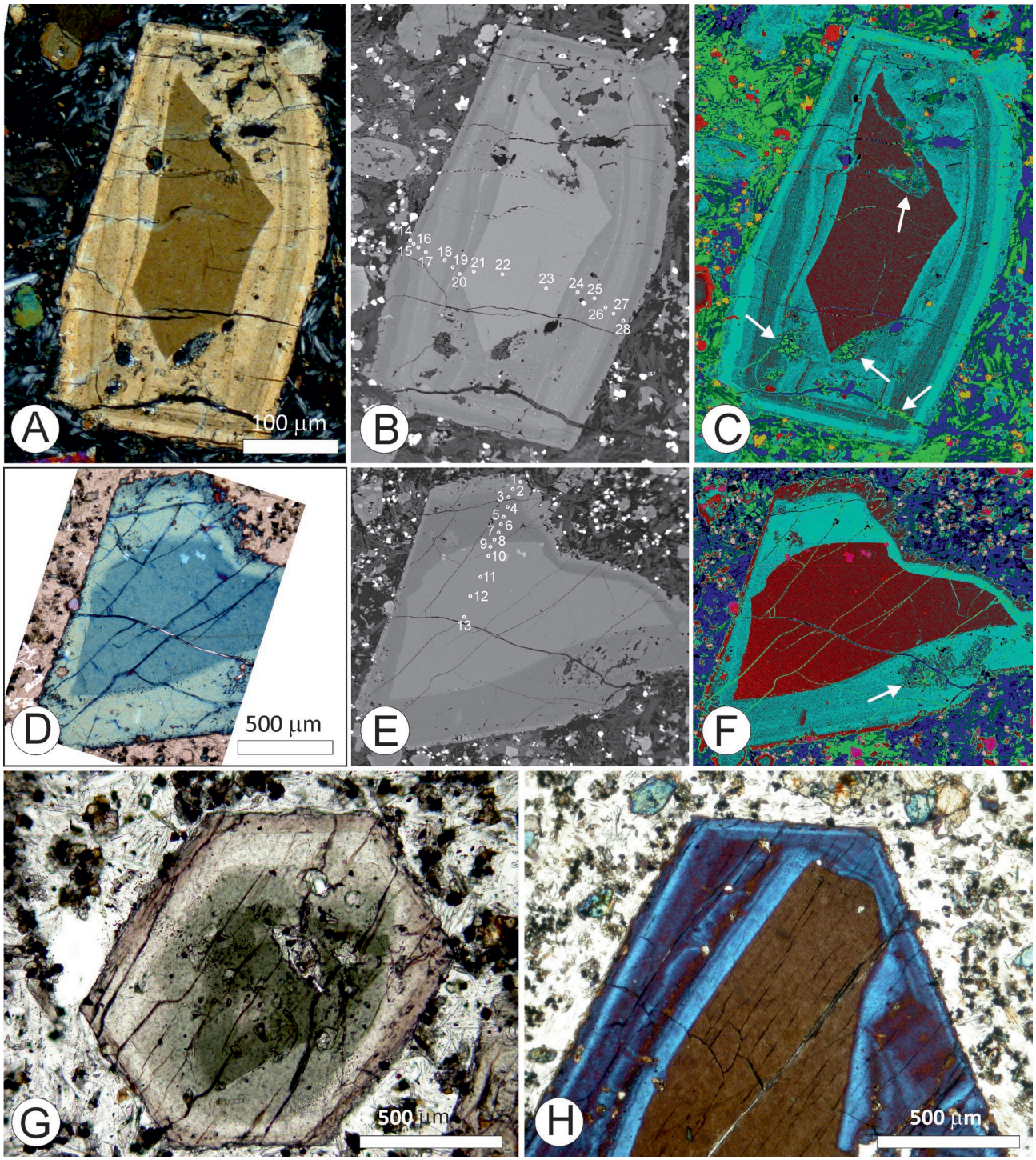

Fig. 3. Oscillatory zoned clinopyroxene phenocrysts with olive-green cores from Mašková (A–F) and Fiľakovské Kováče–Ratka (G–H). **A** — Cross-polarised transmitted light (CPTL) image of irregular, homogeneous, green clinopyroxene core overgrown by oscillatory zoned clinopyroxene rim. **B** — Back-scattered electron (BSE) image of previous grain with EPMA analytical points. **C** — False colour-coded BSE (CC-BSE) image of the same pyroxene with white arrows designating infiltrations of surrounding basalt, which appear green. **D–F** — Zoned clinopyroxene from Mašková with homogeneous xenocrystic core overgrown by rhythmically zoned rim visualized in CPTL (D), BSE (E), and CC-BSE (F). **G** — Plane-polarised transmitted light (PPTL) image of euhedral autocryst with anhedral olive-green core overgrown by pale-green, colour-less and most external brown clinopyroxene. **H** — CPTL image of a portion of a large clinopyroxene autocryst with homogeneous irregular antecrystic core overgrown by oscillatory zoned band. Perfect euhedral shape indicates equilibrium crystallization from the surrounding basalt.

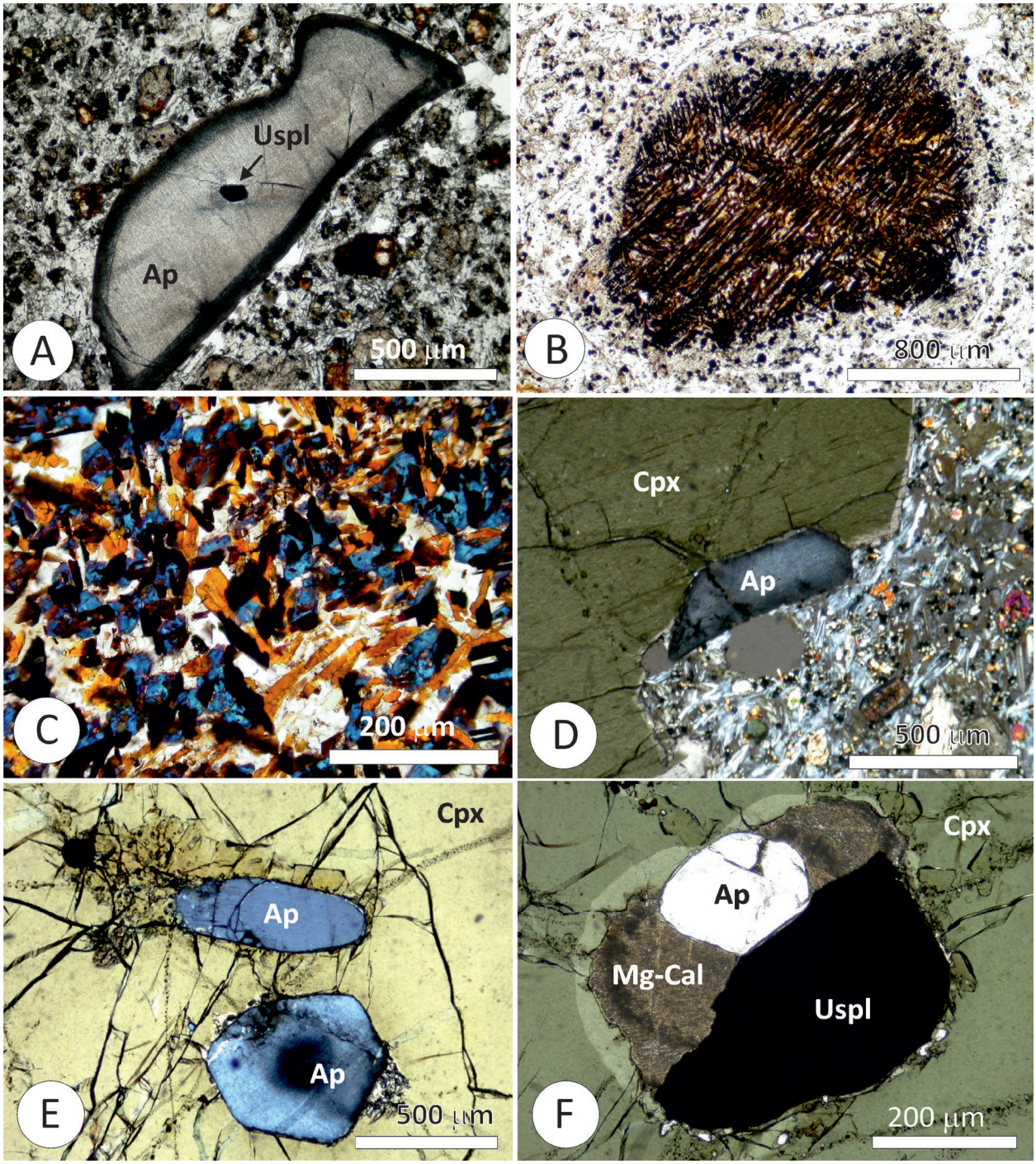

Fig. 4. Megacrystic assemblage with olive-green clinopyroxene megacrysts in Fiľakovské Kováče–Ratka lava flow. **A** — PPTL image of resorbed apatite crystal (Ap) with ulvöspinel inclusion (Uspl). **B** — PPTL image of semi-opaque pseudomorph. **C** — CPTL magnified view of pseudomorph interior composed of olivine (light brown), clinopyroxene (blue), rhönite (black), and white to light-grey interstitial nepheline and plagioclase. **D** — CPTL image of apatite (Ap) intergrown with homogeneous olive-green clinopyroxene (Cpx). **E** — CPTL image of randomly oriented apatite crystals (Ap) in homogeneous clinopyroxene megacryst (Cpx). **F** — PPTL image of a polyphase inclusion of apatite (Ap), ulvöspinel (Uspl), and Mg-calcite (Mg-Cal) with bright reaction band against the clinopyroxene host (Cpx) indicative of a post-entrapment re-equilibration with carbonatite liquid.

Volumetric ratios of pseudomorph phases roughly correspond to Ti-rich magnesio-hastingsite. Mutual intergrowths of ulvöspinel–magnetite series, apatite, olive-green clinopyroxene and opaque pseudomorphs (Fig. 4D) indicate their intimate genetic relationship further underlined by the occurrence of ulvöspinel inclusions in apatite (Fig. 4A), apatite inclusions in clinopyroxene (Fig. 4E), and polyphase inclusions of apatite, ulvöspinel–magnetite and Mg-calcite in the olive-green clinopyroxene (Fig. 4F).

Clinopyroxenes in volcanoclastic deposits occur as dark green to black, almost opaque fragments of prismatic crystals up to 2 mm in diameter. They represent a significant portion of heavy mineral fraction (ca. 50–60 vol. %) accompanied by garnet, amphibole, olivine and rare apatite, zircon, titanite, epidote, tourmaline, spinel, and rutile. The clastic clinopyroxenes are mostly homogeneous except for a portion of grains from Hodejov maar, Tachty and Šurice diatremes, showing oscillatory to sector zoning. Spinel inclusions have been detected in some clinopyroxene grains. Clinopyroxenes have also been studied in Fiľakovo – Červený vrch and Hajnáčka – Kostná dolina maars.

Igneous cumulates

Igneous cumulates originate by the gravitational settling of minerals during magma fractionation and are entrained in later batches of uprising magma as xenoliths. Clinopyroxene and olivine are usually early cumulate minerals, followed by inter-cumulus spinel and post-cumulus Ca-plagioclase and kaersutite–pargasite (Huraiová et al. 1996). Typical compositions of the most abundant mafic xenoliths involve clinopyroxene–olivine–Ca-plagioclase cumulates, clinopyroxene–dominated rocks with minor olivine, spinel, Ca-plagioclase and amphibole (Fig. 5A), and amphibole-dominated rocks with Ca-plagioclase and minor clinopyroxene. In BSE contrast, clinopyroxenes in all mafic cumulates exhibit sector- and oscillatory zoning (Fig. 6).

Unusual mafic cumulates are represented by carbonatized clinopyroxene–apatite–pargasite–phlogopite (Hurai et al. 2007) and spinel–clinopyroxene xenoliths identified in Mašková lava flow. An amphibole–biotite–titanite–ilmenite–plagioclase xenolith devoid of clinopyroxene from the Pinciná maar is crucial for understanding the late evolutionary stages of magma fractionation.

Syenites representing felsic flotation cumulates from evolved magmas have been described from Pinciná maar, Hajnáčka diatreme (Hurai et al. 1998, 2021) and Čamovce–Belinský vrch lava flow (this paper). Clinopyroxene-bearing syenites are dominated by ternary feldspars (Fig. 5B), rarely accompanied by quartz, unzoned augite–hedenbergite and plethora of accessory minerals: apatite, zircon, baddeleyite, zirconolite, yttrialite-Y, britholite-Y, britholite-Ce, chevkinite-Ce, monazite-Ce, rhabdophane, uranothorite, barite, Nb-rutile, ilmenite, and Zr-rich titanite (Hurai et al. 2021). Co-sanguinity of mafic and felsic cumulates formed by the fractional crystallization of mantle-derived mafic magmas has been proven by fluid and melt inclusions (Huraiová et al. 1996), trace element geochemical fingerprints and stable and radiogenic isotopes (Hurai et al. 1998).

Clinopyroxene compositions

All megacrystic and phenocrystic pyroxenes plot in the QUAD field of the Q–J classification diagram (Morimoto et al. 1988) and their compositions extend across Fe-diopside to augite fields in the QUAD (Wo–En–Fs) diagram (Fig. 7). Noteworthy is the compositional similarity of both clinopyroxene sub-types, partly stemming from the fact that complex olive-green core pyroxenes and their oscillatory zoned margins have been sometimes involved in the group of phenocrystic pyroxenes. Both megacrystic and phenocrystic pyroxenes

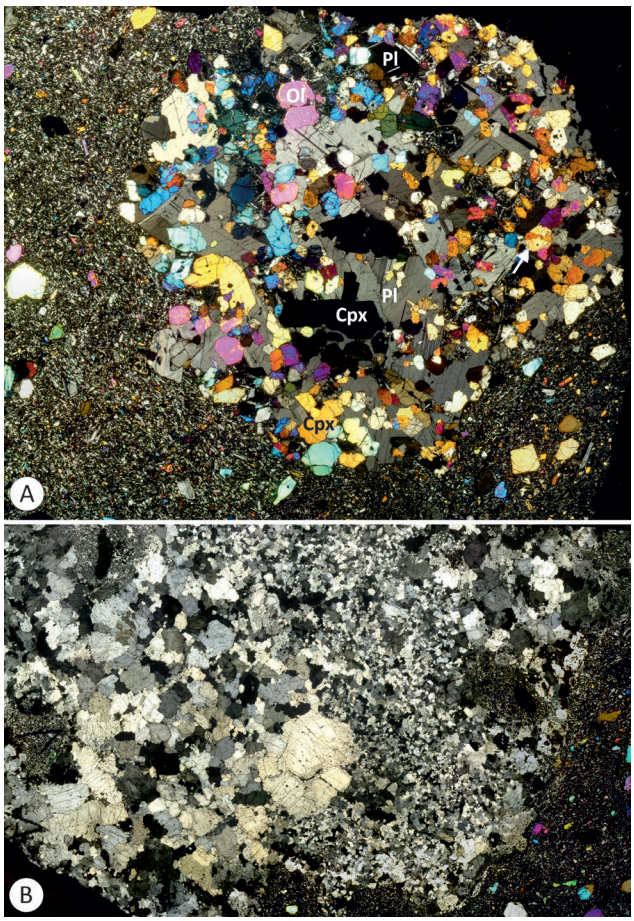

Fig. 5. Composite CPTL images of mafic clinopyroxene–olivine–plagioclase cumulate (**A**) and felsic, diopside-bearing syenite cumulate (**B**) entrained in the Čamovce – Belinský vrch basalt. Some clinopyroxenes in the mafic cumulate show distinct hour-glass zoning (white arrow). Felsic cumulate dominated by recrystallized ternary feldspars contains two finely grained embayments of basalts discernible in the left part of thin section. Widths of views correspond to 4 cm. Mineral abbreviations: Pl – plagioclase, Cpx – clinopyroxene, Ol – olivine.

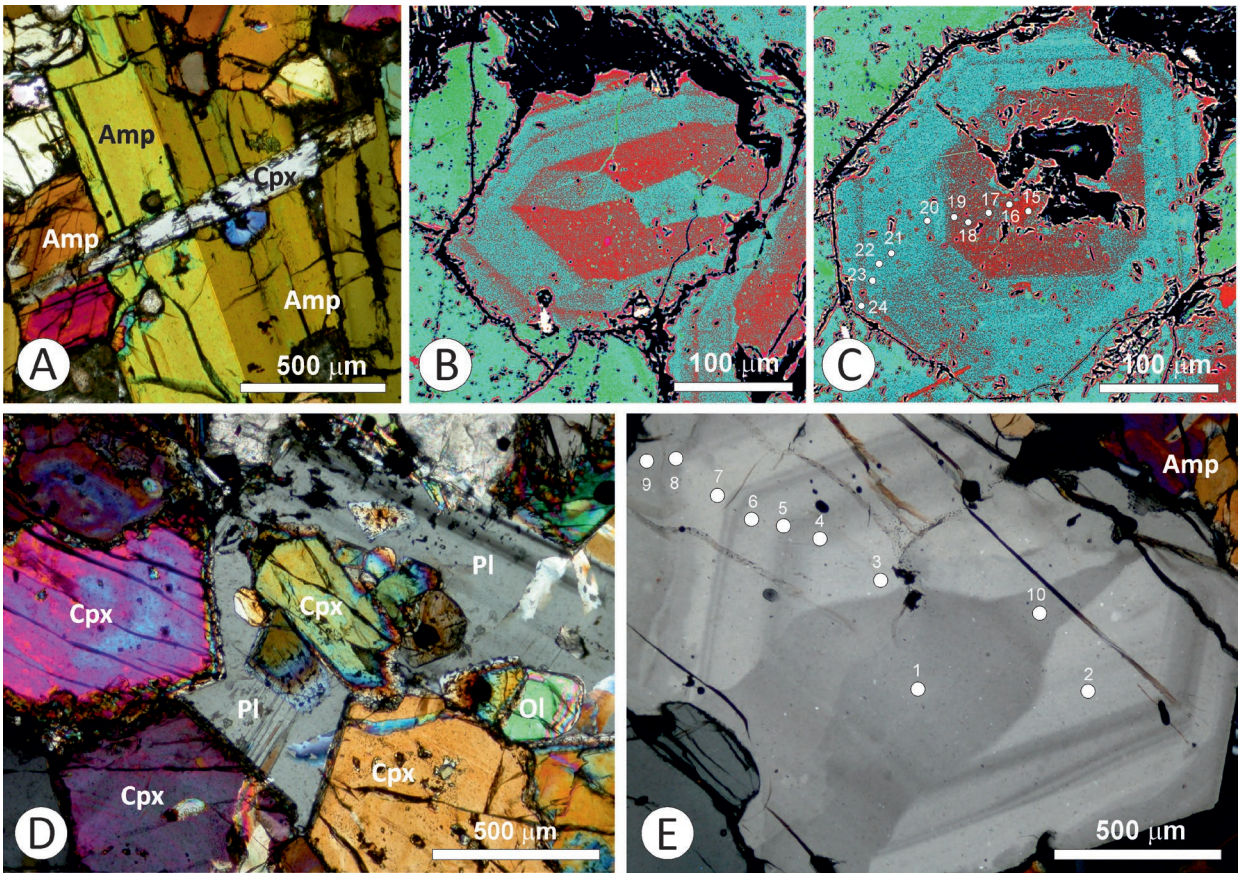

Fig. 6. Typical textures of cumulate xenoliths and internal zoning of clinopyroxenes from Hodejov (A–C), Čamovce (D), and Pinciná (E). **A** — CPTL image of elongate clinopyroxene (Cpx) overgrown by kaersutite (Amp) in hornblendite xenolith. **B** — CC-BSE image of transversal section of clinopyroxene with hour-glass zoning in centre and oscillatory zoning in margins. **C** — CC-BSE image of oscillatory zoned clinopyroxene with hollow in central part. **D** — CPTL image of cumulate clinopyroxene and olivine and post-cumulus interstitial plagioclase (Pl) in gabbroic xenolith. **E** — CPTL image of clinopyroxene from gabbroic xenolith showing combination of hour-glass and oscillatory zoning. Circles and numbers in C and E denote positions of EPMA analytical points.

contain appreciable amounts of aluminium stored in the Ca–Al-tschermakite component. The end-member compositions correspond to augite, aluminian augite, diopside and ferrian–aluminian diopside. Megacrystic clinopyroxenes are ferrian–aluminian diopsides and augites.

Pyroxenes from volcanoclastic deposits also plot in the QUAD field of the Q–J classification diagram and their compositions range from dominant augite and aluminian-augite to less frequent diopside (Fig. 7B). Increased aluminium (2.2–12.8 wt. % Al_2O_3) is bound in the Ca–Al-tschermakite molecule. Mg# numbers defined as $100 \times Mg/(Mg+Fe)$ ratios are scattered in the interval from 78 to 98 that is narrower than that recorded in clinopyroxene megacrysts and phenocrysts. Most volcanoclastic clinopyroxenes are also titanium-rich, with up to 5.2 wt. % TiO_2. In contrast, low-Ti clinopyroxenes with less than 0.5 wt. % TiO_2 from the Gemerské Dechtáre maar contain increased Cr contents, up to 1 wt. % Cr_2O_3. The low-Ti, high-Cr clinopyroxenes also occur in volcanoclastic deposits of Hajnáčka – Kostná dolina and Hodejov maars, and Tachty diatreme.

Clinopyroxenes from mafic cumulate xenoliths plot within the QUAD field and along the QUAD–Ca-tschermakite join, being thus quite similar to volcanoclastic clinopyroxenes (Fig. 8). Green clinopyroxenes in syenite xenoliths from Hajnáčka diatreme project within the hedenbergite field. Clinopyroxenite cumulates from Tri Chotáre and Čamovce display increased Cr concentrations, 0.8–1.2 wt. % Cr_2O_3, accompanied by low TiO_2 contents (0.3–1.3 wt. %). Clinopyroxenes in remaining cumulates are typically Cr-poor, with Cr_2O_3 concentrations <0.5 wt. % and variable TiO_2 contents reaching up to 4.5 wt. %.

Correlation diagram based on Mg# and Ti# numbers reveals two distinct substitution vectors (Fig. 9A). The first vector with sharply decreasing Mg# and almost fixed Ti# ($100 \times Ti/(Ti+Al+Cr)$) is typical for homogeneous megacrysts and resorbed antecrystic cores of zoned phenocrysts. The second vector characterized by Ti# sharply increasing from 10 to 25 and concomitantly moderately decreasing Mg# from ~85 to ~70 is typical for oscillatory zoned clinopyroxenes. Compositions of clinopyroxenes from cumulates cluster around

Mg# ~85 and Ti# ~10, close to the intersection point of both vectors (Fig. 9B). Four clinopyroxene fragments from volcanoclastic deposits overlap the megacrystic trend and can thus be unequivocally affiliated with antecrysts genetically unrelated with their basalt host. Volcanoclastic clinopyroxenes with Ti# <10 are probably xenocrystic fragments scavenged from the mantle because they overlap the compositions of clinopyroxenes in spinel peridotite xenoliths.

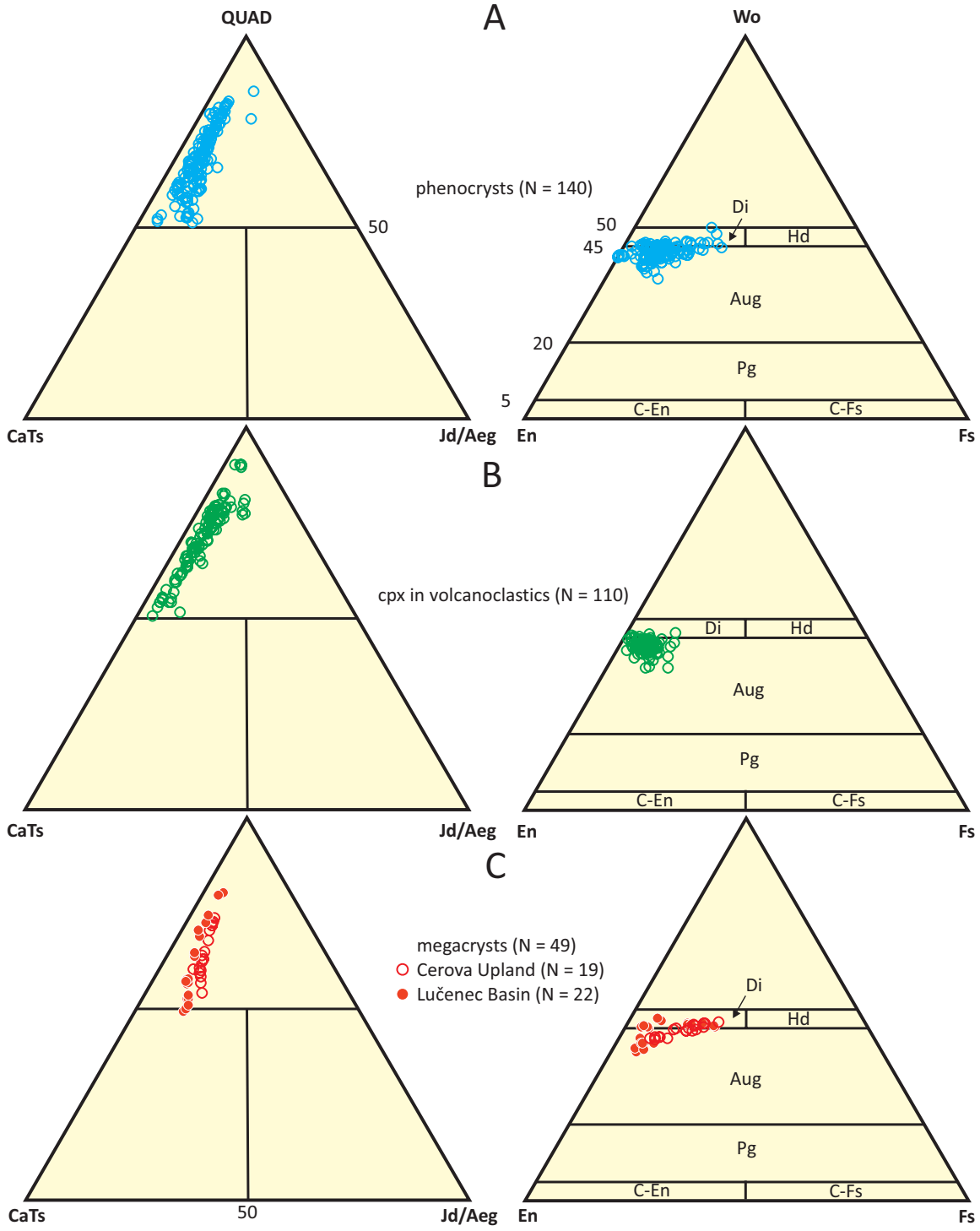

Fig. 7. Compositional classification diagrams of clinopyroxene phenocrysts and megacrysts in basalts and clastic clinopyroxenes in volcanoclastic deposits. Mineral abbreviations: Wo – wollastonite, En – enstatite, Fs – ferrosilite, CaTs – Ca-tschermakite, Jd – jadeite, Aeg – aegirine, Di – diopside, Hd – hedenbergite, Aug – augite, Pg – pigeonite, C-En – clinoenstatite, C-Fs – clinoferrosilite, QUAD – Wo+En+Fs. Numbers denote mole percentages of endmembers. Numbers in parentheses denote analytical frequency.

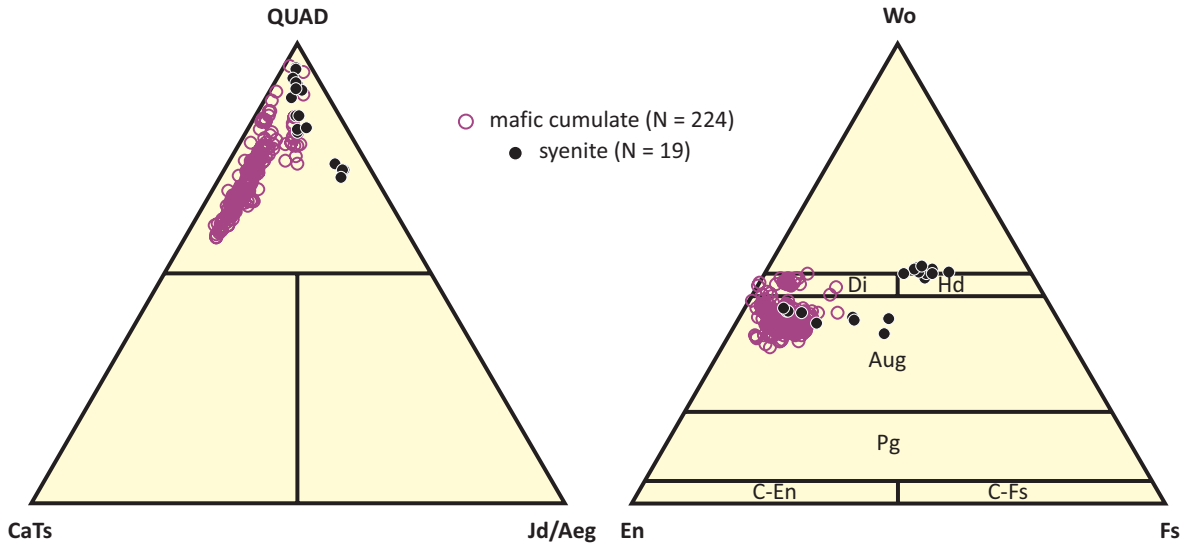

Fig. 8. Compositional classification diagrams of clinopyroxenes from cumulate xenoliths. Numbers in parentheses denote analytical frequency. Mineral abbreviations as in Fig. 7.

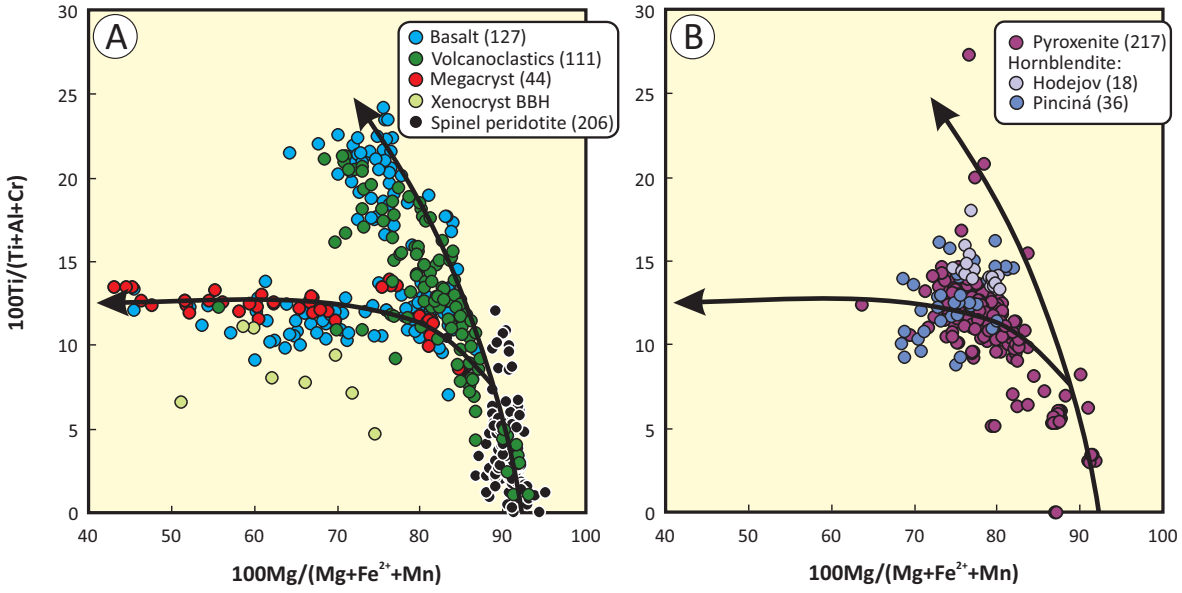

Fig. 9. Correlation between Mg# and Ti# numbers in megacrysts and phenocrysts of basalts, volcanoclastics (**A**) and mafic cumulates (**B**), showing two different substitution vectors indicated by arrows. Data on clinopyroxenes from spinel peridotite xenoliths (Konečný 2005) and green clinopyroxene xenocrysts of Bakony–Balaton Highland Basalts (BBH) from the western part of Pannonian Basin (Jankovics et al. 2016) are also displayed in A.

Chemical and geotectonic discrimination

Ca, Na, Ti, Cr and Al contents determined by EPMA enable, with greater than 80 % confidence, discrimination among various types of magmatic clinopyroxenes crystallizing from: (1) alkali basalts, basanites and their derivatives from oceanic or continental intra-plate settings; (2) non-orogenic tholeiites and transitional basalts from spreading zones, rifts, back-arc basins, oceanic islands and passive continental margins; (3) orogenic calc-alkalic or tholeiitic basalts from active continental margins and island arcs (Leterrier et al. 1982). In accord with expectations, the majority of clinopyroxene phenocrysts, fragments and homogeneous megacrysts of SSB basalts plot within the field of parental alkali basalts and their derivatives, whereas the non-alkalic affinity exhibits only subordinate part of investigated crystals and fragments

(Fig. 10). Clinopyroxenes from mafic cumulate xenoliths exhibit both alkalic and non-alkalic affinities, showing a larger proportion of transitional types plotting on both sides of the division line between the two groups. Only few clinopyroxenite samples, two from Čamovce-Belinský vrch and one from Tri Chotáre, are unequivocally non-alkalic. Transitional types occur in Pinciná, Fiľakovské Kováče and Čamovce–Belinský vrch, whereas volcanic structures of Dunivá Hora, Gortva, Hodejov, Mačacia in Cerová Upland, and Mašková in Lučenec Basin contain only alkalic mafic xenoliths. The Pinciná maar contains mafic cumulate xenoliths of both alkalic and transitional types; whereas all three categories occur in the Čamovce–Belinský vrch lava flow.

The non-alkalic clinopyroxenes can further be discriminated using diagrams correlating Ca and Ti+Cr contents (Fig. 11). Most non-alkalic clinopyroxenes from volcanoclastic deposits of the SSB project within the field of non-orogenic, MORB-like tholeiites or very close around the division line with supra-subduction magmas, except for just two fragments from the Gemerské Dechtáre maar, unequivocally falling deep within the field of supra-subduction parental melts. All non-alkalic clinopyroxenes from mafic cumulates fell invariantly within the field of non-orogenic tholeiites or very close to the division line separating them from supra-subduction magmas.

Single-pyroxene thermobarometry

Compositional profiles across zoned clinopyroxenes revealed almost homogeneous olive-green Al- and Fe-rich megacrystic cores surrounded by Mg-rich oscillatory zoned

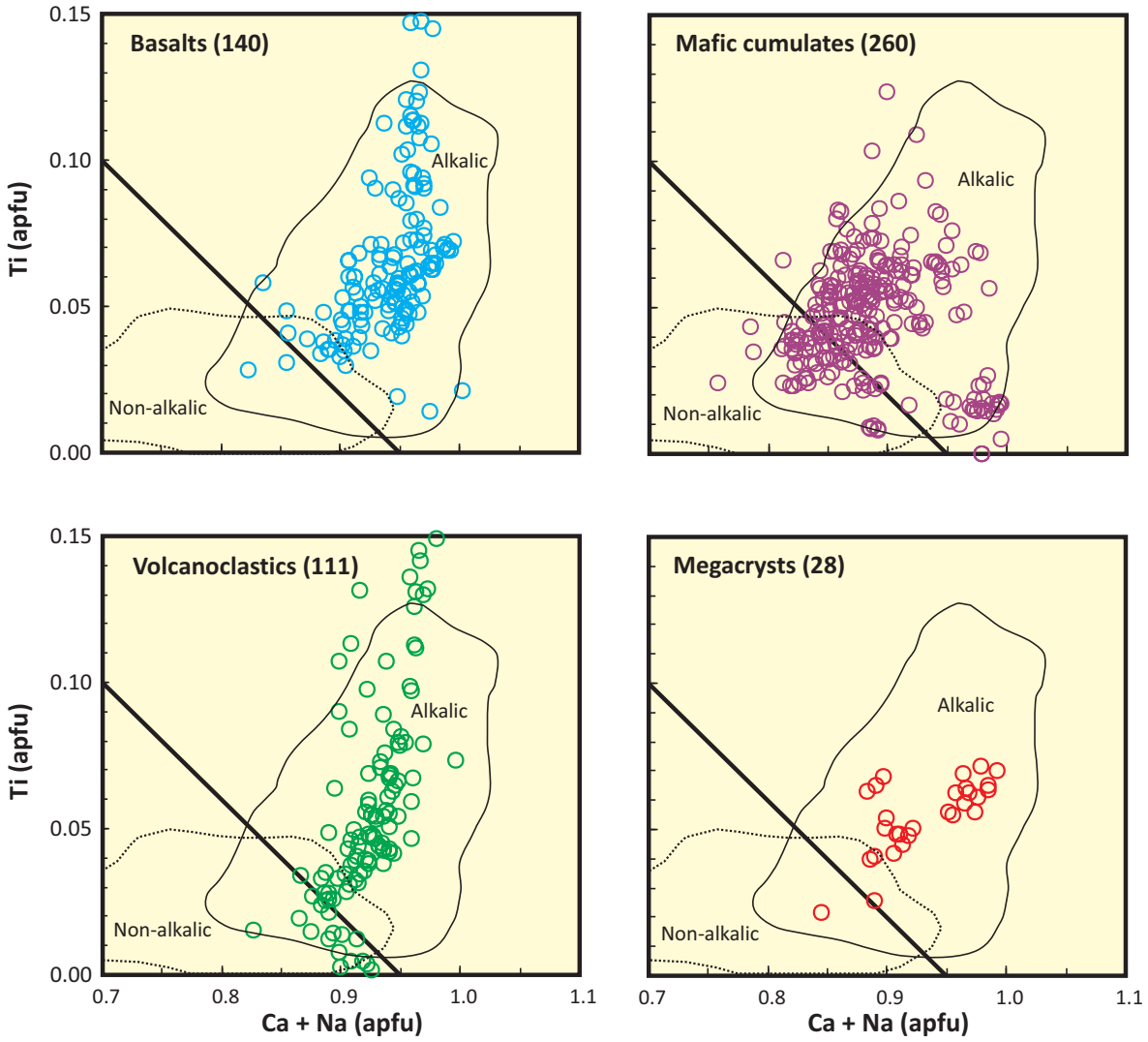

Fig. 10. Ca+Na versus Ti discrimination diagrams (Leterrier et al. 1982) with projection points of phenocrysts in basalts, mafic cumulates, clinopyroxene fragments in volcanoclastics, and megacrystic clinopyroxenes. Thick oblique lines discriminate alkalic from non-alkalic (tholeiitic or calc-alkalic) parental melts. Contoured are boundaries of 86 % confidence level for alkalic (solid curve) and 92 % confidence level for non-alkalic (stippled curve) clinopyroxenes. Numbers in parentheses denote analytical frequency.

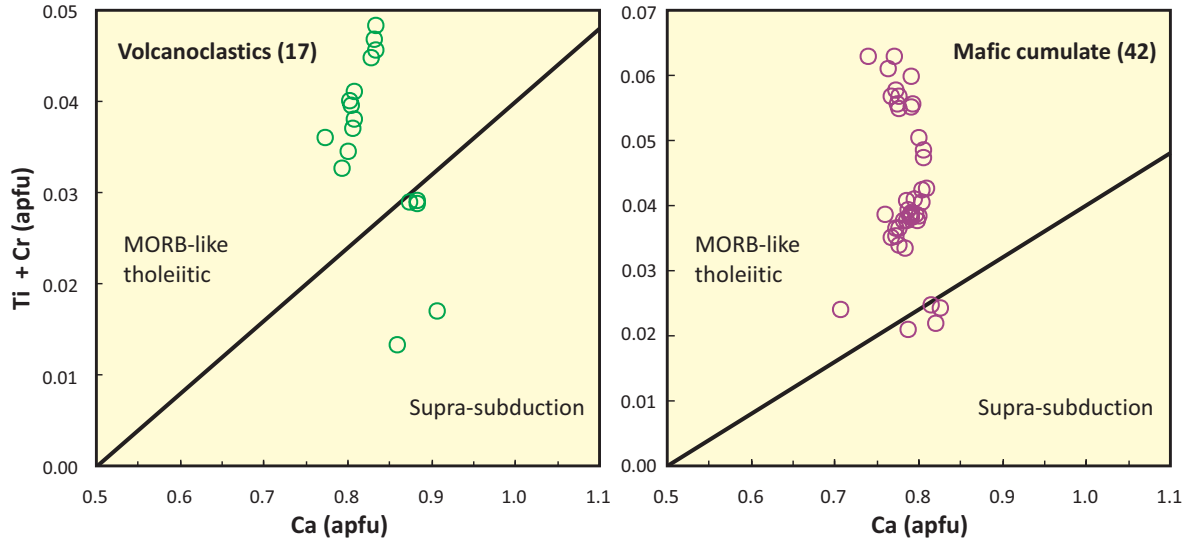

Fig. 11. Ca versus Ti + Cr discrimination diagram for non-alkalic clinopyroxenes (Leterrier et al. 1982) with data from clinopyroxene fragments in volcanoclastic deposits and mafic cumulates. Thick oblique line discriminates supra-subduction (orogenic) and MORB-like tholeiitic basalts. Numbers in parentheses denote analytical frequency.

rims (Fig. 12). Thermobarometric data indicate lower equilibration temperature of the homogeneous cores, typically 1000–1070 °C, and higher pressures (0.84–1.21 GPa), compared to oscillatory zoned rims, which exhibit temperatures of 1075–1140 °C and pressures of 0.64–1.0 GPa at the base of the oscillatory zoned part close to the interface with megacrystic cores. The oscillatory zoned parts of composite phenocrysts exhibit competing temperatures and pressures generally decreasing towards phenocryst margins. Care should be, however, exerted to interpret *P–T* data from olive-green cores with Mg# numbers often below the acceptable limit of 70 required for the safe application of single-pyroxene thermobarometry.

Compositional profiles across clinopyroxenes from mafic cumulate xenoliths also document competing behaviour of Mg against Al and Fe (Fig. 12), thus reflecting episodes of steady-state equilibrium crystallization interrupted by an abrupt pressure release and temperature increase caused likely by the replenishment of the magmatic reservoir. The same mechanism accounts most likely for the competing Mg and Fe+Al contents in oscillatory zoned phenocrysts.

Some zoned clinopyroxene grains from mafic cumulates also show compositional perturbations around hollows and grain boundaries (Fig. 6C), indicating a non-equilibrium element exchange with percolating fluids or melts. Hence, smaller xenoliths or clinopyroxene fragments are more susceptible to recording erratic *P–T* conditions during accelerated ascent to the surface. The perturbation due to percolating fluid or melt can be distinguished from magmatic replenishment episodes by the Mg depletion.

Figure 13 summarizes *P–T* data from phenocrysts, megacrysts and clinopyroxene-bearing mafic cumulates. The volcanoclastic clinopyroxene autocrysts mostly follow a cooling trajectory propagating from 1351 °C and 2.16 GPa to ~1000–1100 °C and ~0.1 GPa. Small sub-group of clastic clinopyroxenes of tholeiitic affinity is shifted to somewhat higher temperatures (1170–1351 °C) compared to clinopyroxenes of alkalic affinity (1000–1250 °C), which returned lower pressures (<1.21 GPa).

In line with our expectations, *P–T* data from oscillatory zoned phenocrysts from basalts overlap the field of clinopyroxenes with alkalic affinity from volcanoclastic deposits. Interestingly, however, clinopyroxenes with the tholeiitic MORB-like affinity have not been detected in effusive basalts. Here in contrast, clinopyroxenes plotting outside the autocrystic field down to 980 °C and pressures up to 1.5 GPa are rather abundant. All these clinopyroxenes are characterized by Ti# <15 diagnostic for olive-green antecrysts. Their formation *T–P* conditions, 980–1230 °C and 0.6–1.5 GPa, overlap of the autocryst field at the high-*T* end.

The highest equilibration temperatures have been recorded in a clinopyroxene cumulate with tholeiitic affinity from Tri Chotáre (1342 °C, 1.98 GPa). Another clinopyroxenite xenolith with tholeiitic affinity from Čamovce – Belinský vrch returned 1197–1230 °C and 0.81–1.0 GPa. Transitional clinopyroxenite cumulates also yielded *P–T* parameters comparable to tholeiitic types, ranging at 1115–1297 °C and 0.71–2.07 GPa.

Somewhat more complicated picture is provided by mafic cumulates of alkalic affinity. Their *P–T* data roughly overlap the field of autocrystic clinopyroxenes, however, pressures less than 0.65 GPa have been returned by just one clinopyroxenite xenolith from Mašková basalt. The broad data dispersion together with 23 % rejection rate of analyses with bad stoichiometry indicates compositional perturbations caused by the non-equilibrium interaction of the xenolith with fluids or

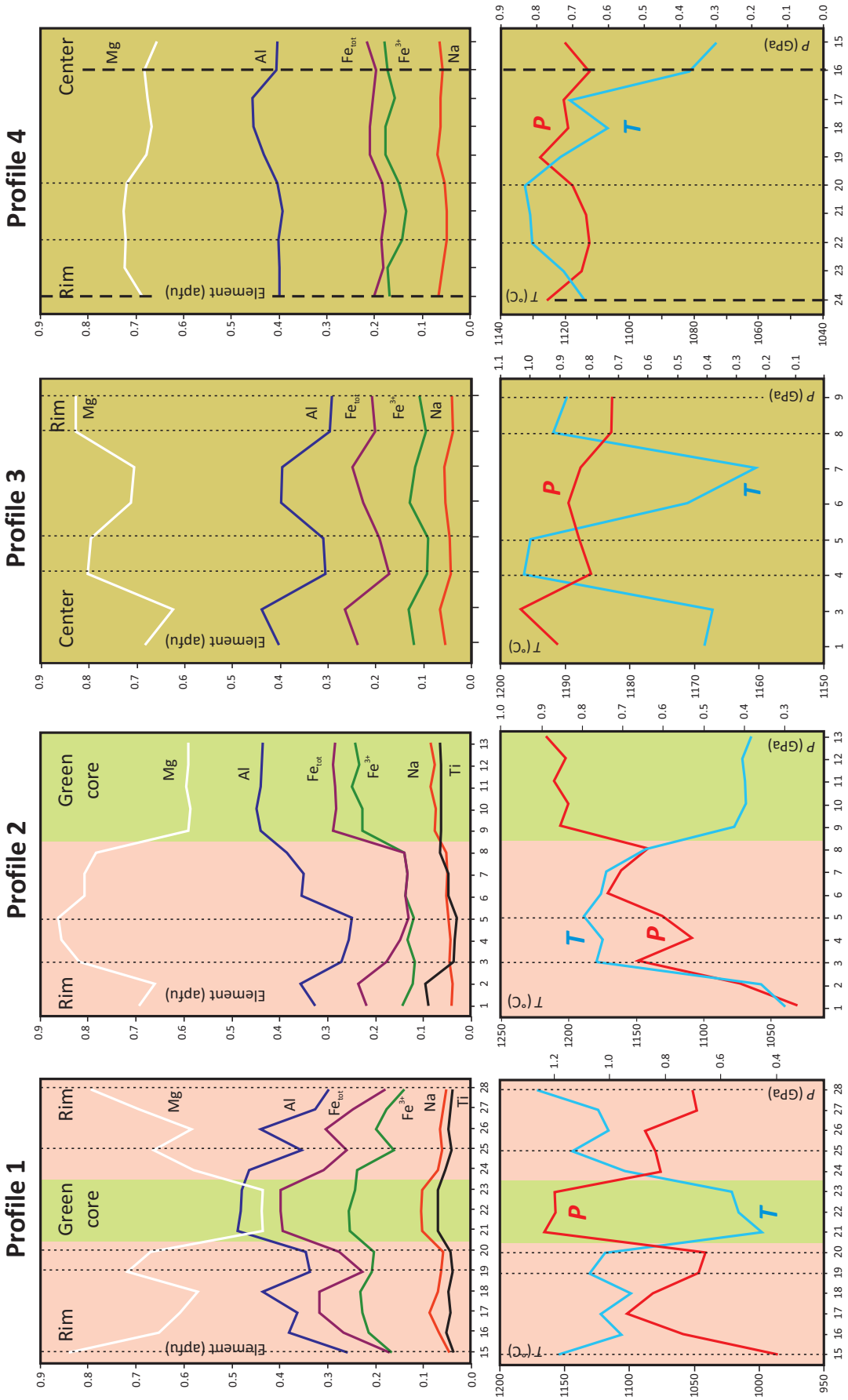

Fig. 12. Compositional and thermobarometric (*T–P*) profiles of zoned green-core clinopyroxene phenocrysts from Mašková (Fig. 3A–C, Profile 1 and 3D–F, Profile 2), zoned clinopyroxenes in gabbro cumulate from Pinciná (Fig. 6E, Profile 3) and zoned clinopyroxene in hornblendite cumulate from Hodejov (Fig. 6C, Profile 4). Replenishment episodes and perturbations due to percolating fluids or melts are marked by thin short-dashed and thick long-dashed vertical lines, respectively.

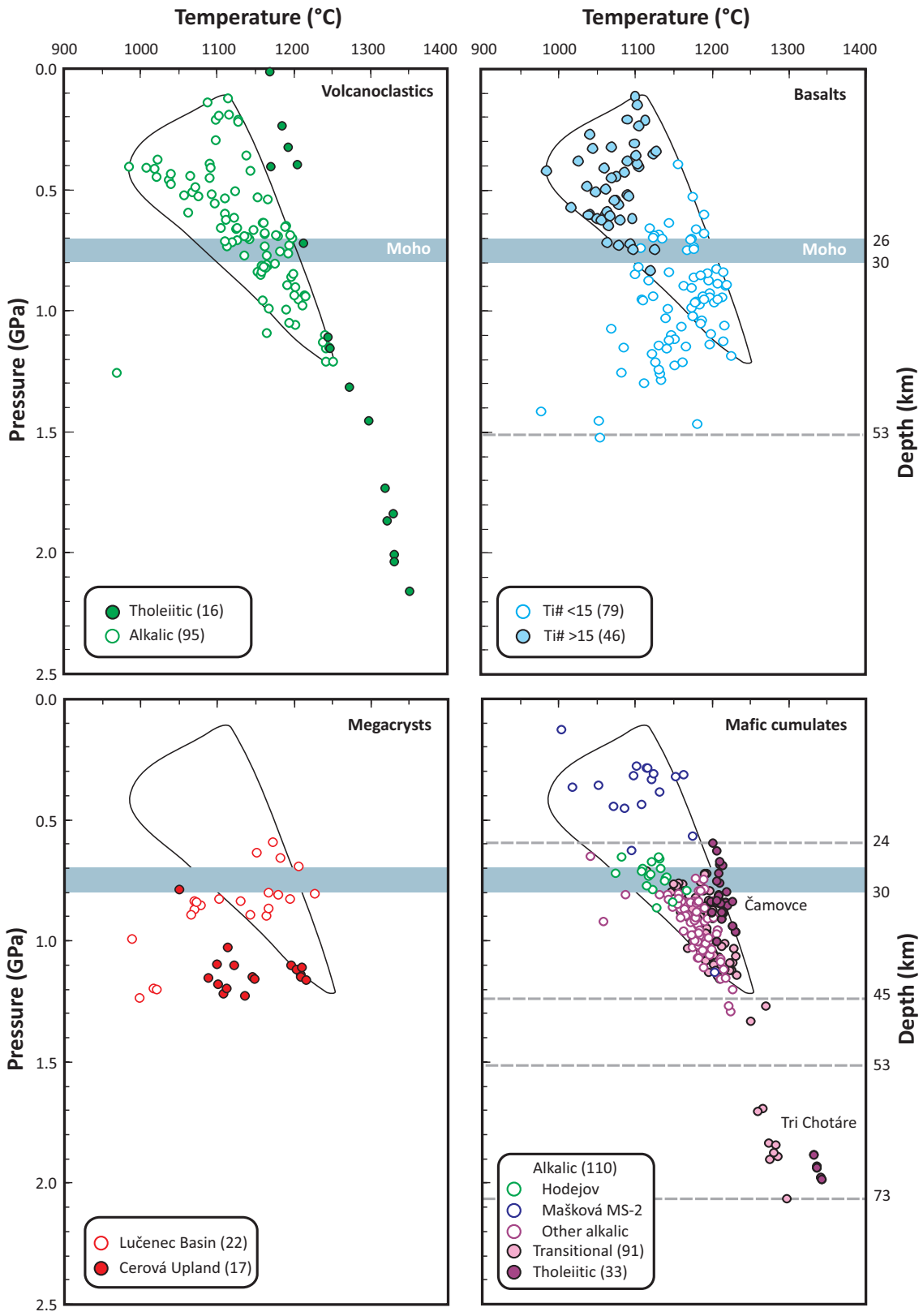

Fig. 13. Clinopyroxene thermobarometry data obtained from mafic cumulates, megacrysts, and phenocrysts in basalts and volcanoclastic deposits of the SSB. Depths (h) equivalent to lithostatic load were calculated from pressures using the equation: $h = P/D \times g$, where P is pressure [in 10^5Pa = 1 bar = 0.0001 GPa], D is density of an average continental crust (2750 kg.m^{-3}) and the mantle (3200 kg.m^{-3}), g is acceleration due to gravitation (9.81 m.s^{-2}). Numbers in parentheses denote analytical frequency for given dataset. Only analyses with analytical totals between 98 and 102 wt. %, 2T- and 2M-site cations, and $Mg/Mg+Fe^{2+} > 0.7$ have been involved in thermobarometry.

melts. Other mafic cumulates with alkalic affinity returned pressures from 0.65 to 1.29 GPa, and temperatures between 1041 and 1226 °C.

Dissussion

Parental melts of igneous cumulates

Cumulate xenoliths are valuable sources of genetic information encrypted in assemblages of coexisting minerals, which can be reproduced using thermodynamic modelling. Clinopyroxene is the first phase to crystallize from less alkalic basalts at increased pressures (e.g., Fujii & Kushiro 1977), thus carrying information about pre-eruptive water contents of parental melts. The water contents dissolved in basalt melt can be estimated either from thermodynamic models or directly measured in high-temperature clinopyroxenes by infrared spectroscopy (Kovács et al. 2020). This information can further be employed to constrain the mantle melting and basalt fractionation models.

It should be emphasized that the tholeiitic affinity of cumulate clinopyroxenes inferred from minor elements is inconsistent with the associated mineral assemblage containing olivine and devoid of orthopyroxene, thus reflecting a silica-unsaturated alkalic, rather than silica-oversaturated sub-alkalic melt precursor. On the other hand, the absence of foids, namely nepheline and sodalite along with plagioclases in the post-cumulus assemblage of mafic xenoliths as well as flotation cumulates rules out strongly alkalic parental melts. Hence, it seems reasonable to select from the dataset of SSB basalts those with low-to-moderate alkali contents as candidates for cumulate parental melts and to utilize their compositions as input parameters for thermodynamic modelling. Basanite from Konrádovce and basalt from Šurice, with alkalinity indices IA corresponding to 2.0 and 3.8 and Mg# numbers 50 and 51, respectively, have been selected as prospective parents of mafic cumulates with transitional and "tholeiitic" affinities, respectively, owing to their high Mg and low Si contents. Basanite from Guda (IA = 5, Mg# = 44) was chosen as a template for modelling the fractionation of more alkalic melts.

In the first step, single-pyroxene thermobarometric data have been overlapped by clinopyroxene liquidi constructed from pseudosections constrained by compositions of Konrádovce basanite and Šurice basalt. In the second step, pseudosections have been calculated for the average calculated water contents for the whole range of temperatures (900–1400 °C) and pressures (0.5–2 GPa) to cover the presumable cooling trajectory of basalts ascending from the partial melting zone and stalling below Moho.

Clinopyroxenes from transitional and "tholeiitic" cumulate xenoliths plot between 1 and 2 wt. % isopleths constrained by pseudosections (Fig. 14) and the estimated respective water contents correspond to 1.4±0.1 and 1.16±0.04 wt. % H_2O. The Šurice model applied to volcanoclastic clinopyroxenes of "tholeiitic" affinity returned 1.4±0.2 wt. % H_2O. The estimated

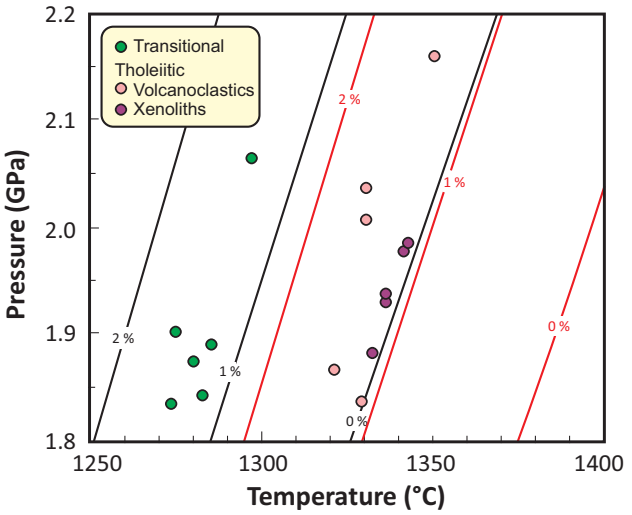

Fig. 14. Enlarged view of high-*PT* part of the KNCMFATSHO system constrained by compositions of Konrádovce basanite (black lines) and Šurice basalt (red lines), with isopleths of water contents (wt. % H_2O) dissolved in the melt along clinopyroxene liquidi. Circles are projection points of maximum *P–T* parameters provided by clinopyroxenes from mafic cumulate xenoliths and volcanoclastics.

water contents are somewhat lower than the range of 2–2.5 wt. % H_2O inferred from structural hydroxyl contents of clinopyroxenes in alkali basalts from Bakony–Balaton Highland Volcanic Field of central Hungary (Kovács et al. 2020).

Expanded, yet simplified pseudosections of Šurice, Konrádovce and Guda basalts with 1, 1.5 and 2 wt. % dissolved water are shown in Fig. 15, together with presumable cooling trajectories constructed from clinopyroxene thermobarometric data. The concave shape of the trajectories reflects initially near-adiabatic ascent of the basaltic magma from the zone of partial melting at pressures greater than 2 GPa, decceleration due to onset of intense crystal accumulation in the upper lithospheric mantle and nearly isobaric cooling in stagnant reservoirs located below Moho at pressures around 0.65 GPa.

The model of Šurice basalt with 1 wt. % H_2O and the estimated cooling trajectory (Fig. 15A) satisfactorily overlaps the clinopyroxene thermobarometric data, but is inconsistent with the presence of cumulate olivine associated with clinopyroxene. The model, however, well reproduces the crystallization of intercumulus spinel and post-cumulus amphibole–plagioclase at temperatures below 1050 °C from 20–50 vol. % silicate melt fraction remaining in the system. The Šurice model also predicts the titanite–ilmenite–biotite–amphibole–plagioclase assemblage detected in one xenolith from the Pinciná maar. The assemblage was stable in the temperature interval from 900 to 920 °C at 0.65 GPa, with >90 vol. % melt crystallized.

Thermodynamic model of the Konrádovce basanite dissolving 2 % H_2O documents how subtle variations in water contents and alkalinity significantly influence the stability of various mineral assemblages (Fig. 15B). Titanite is no longer

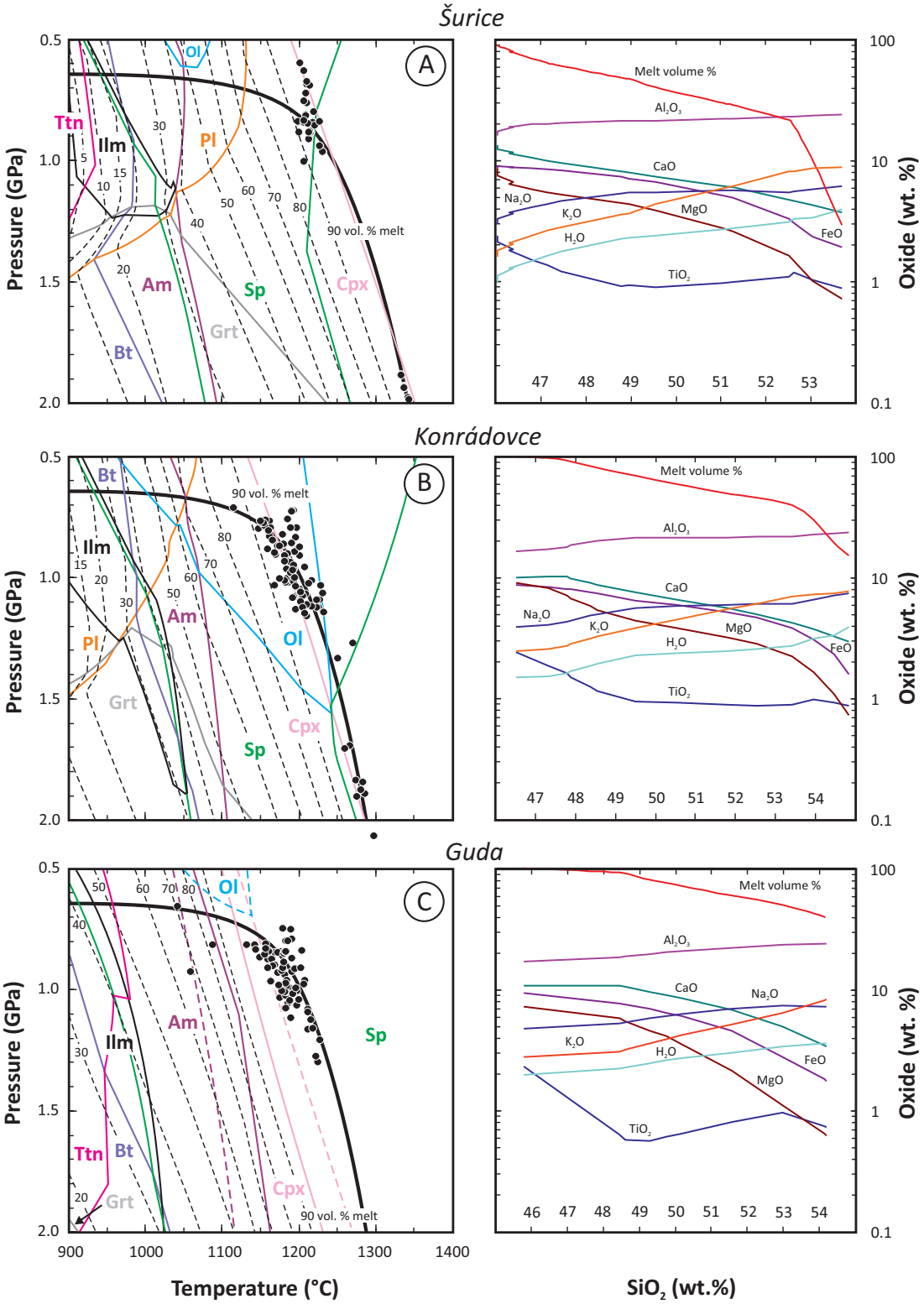

Fig. 15. Left column: Simplified pseudosections constrained by bulk compositions of Šurice, Konrádovce and Guda basalts (Supplementary Table S1) with isolines of volume percentages of melt fraction (dashed curves) and stability fields of following mineral phases: Am – amphibole, Bt – biotite, Cpx – clinopyroxene, Grt – garnet, Ilm – ilmenite, Ol – olivine, Pl – plagioclase, Sp – spinel group minerals, Ttn – titanite. Solid circles are projection points of clinopyroxene thermobarometric data from cumulate xenoliths of "tholeiitic" (**A**), transitional (**B**) and alkalic (**C**) affinities. The diagram in C depicts phase boundaries calculated for 2 wt. % H_2O (solid lines) and 1 wt. % H_2O (stippled lines). Right column: Harker´s diagrams of melt compositions and their volume fractions along cooling trajectories depicted by thick solid curves in the corresponding pseudosections.

present, and plagioclase stability is shifted to lower temperatures. Olivine field is expanded to higher pressures and replaces clinopyroxene at liquidus at <1.4 GPa. The Konrádovce model very well reproduces textural features of most SSB cumulate xenoliths: clinopyroxene and olivine (possibly also titanomagnetite), as early cumulus phases postdated by intercumulus Mg–Al–Fe spinel and poikilitically intergrown, post-cumulus amphibole and plagioclase crystallized simultaneously at ~1050 °C. The volume of residual melt at this stage, ~70 vol. %, is still sufficient to effective crystal separation and formation of honblendite–plagioclase cumulates.

The model of Guda basanite with 2 wt. % H_2O documents, how the increased alkalinity of 5 IA supresses the crystallization of plagioclase and olivine, which are no longer present as stable phases along the estimated cooling trajectory. Moreover, the clinopyroxene melting curve is shifted to lower temperatures, thus leaving outside literally all thermobarometric data (Fig. 15C). Reduction of bulk water content to 1 wt. % stabilizes the plagioclase at the expense of titanite and expands the olivine stability region, which, however, restricted to lower pressures does not intersect the cooling trajectory. Moreover, inhibition of amphibole growth due to depletion in water results in excess of alkalis and the crystallization of nepheline in final stages of crystal accumulation at temperatures around 900–950 °C. Even with the substantially reduced water content, most single-clinopyroxene thermobarometric data plot outside the clinopyroxene stability region. Noteworthy is the large expansion of the stability field of spinel-group minerals, which become liquidus phases up to temperatures higher than 1400 °C. Although inapplicable to most SSB cumulate xenoliths, the Guda model could be helpful in explaining the existence of the rare spinel-clinopyroxene cumulate in the Mašková lava flow, probably documenting more alkalic parental melts.

In summary, analysis of pseudosections showed that moderately alkaline basanite melt was the most plausible precursor of the majority of SSB cumulate xenoliths. This conclusion is consistent with the previous study (Zajacz et al. 2007) based on the investigation of polyphase silicate melt inclusions in olivine from clinopyroxene-olivine cumulates combined with the modelling with pMELTS. Local perturbations in mineral compositions could be explained in terms of changing water contents and alkalinity, fluctuating in a narrow range of 1–2 wt. % H_2O and 3–4 IA, respectively. Formation of ilmenite–titanite–biotite–plagioclase cumulates ejected in the Pinciná maar documents either calc-alkalic basalt precursor, or the assimilation of carbonates in more common, moderately alkaline basalt, or mixing with carbonatite melt. Thermodynamic modelling showed that clinopyroxenes of alkalic and tholeiitic affinities can be produced by the crystallization from moderately alkalic intra-plate basalts.

Fractionation of alkali basalts

Variations in chemical composition of residual melts along cooling trajectories deduced from single-pyroxene thermobarometry are shown in Fig. 15 and Supplementary Table S3. With progressive crystallization of solid phases, Ti, Ca, Mg, and Fe contents decrease, and Al, Si, K, and Na contents increase in residual melts. Ti and Mg are preferentially removed from the melt at higher temperatures, due to accumulation of spinel-group minerals at early fractionation stages. The crossover of K_2O and Na_2O concentration curves reflects the formation of strongly potassic melts during advanced crystal fractionation, with 30–40 vol. % of the silicate liquid remaning in the system. Similar high-K silicate melts have been recorded in polyphase silicate-carbonate inclusions trapped in a clinopyroxenite cumulate xenolith from Mašková lava flow (Hurai et al. 2007).

Fractionation trends calculated for Konrádovce, Šurice and Guda basalts projected through SiO_2 contents, Mg# numbers and aluminium saturation index A/NKC (Fig. 16) overlap compositions of other SSB basalts, which also show inversely correlated Mg and Al contents typical of fractionated magmas. Hence, the whole spectrum of basalt compositions erupted in the SSB can be reproduced by the fractionation from basalts with A/NKC between 0.55 and 0.61, Mg# around 50, SiO_2 concentrations between 46 and 46.5 wt. %, and IA indices 2.0–3.8. It is reasonable to anticipate that all magmas reaching the surface experienced compositional transformations during several episodes of crystal accumulation coincidental with the stalling periods along density boundaries in the mantle and along the mantle-crust boundary. The increased alkalinity of basalts erupted on the surface compared to deep-seated basalt cumulates is also documented by a higher proportion of clinopyroxenes with non-alkalic ("tholeiitic") affinity in the latter (Fig. 10). In particular, high-alkali basalts believed to be generated by a low-degree partial melting of the mantle would be susceptible to significant Ti and Mg depletion due to separation of spinel-group minerals in early stages of crystal fractionation after crossing the basalt liquidus (Fig. 15C). It seems thus improbable that pristine magmas entirely unaffected by crystal accumulation could reach the surface. Our calculations thus provide an alternative to the model of Bracco Gartner & McKenzie (2020), who inferred from forward modelling of major and trace element contents that less than 1 vol. % of the mantle melting is required at a temperature of ~1260 °C at a depth of ~65 km along the lithosphere-asthenosphere boundary (LAB) to reproduce compositions of alkali basalts erupting on surface in the Carpathian–Pannonian realm.

Origin of olive-green megacrysts

Olive-green ferrian–aluminoan augites (named fassaitic augite in earlier works) from Fiľakovské Kováče quarry have been interpreted as antecrysts of evolved alkalic melts mixed with basaltic magma, whereas grass-green Al-diopside (designated as salite and ferrosalite in earlier works) megacrystic cores in zoned phenocrysts have been attributed to wall-rock xenocrysts scavenged from the upper mantle by the ascending basalt and originating from highly evolved magma (Dobosi 1989; Dobosi & Fodor 1992). Szabó & Bodnar (1998) argued

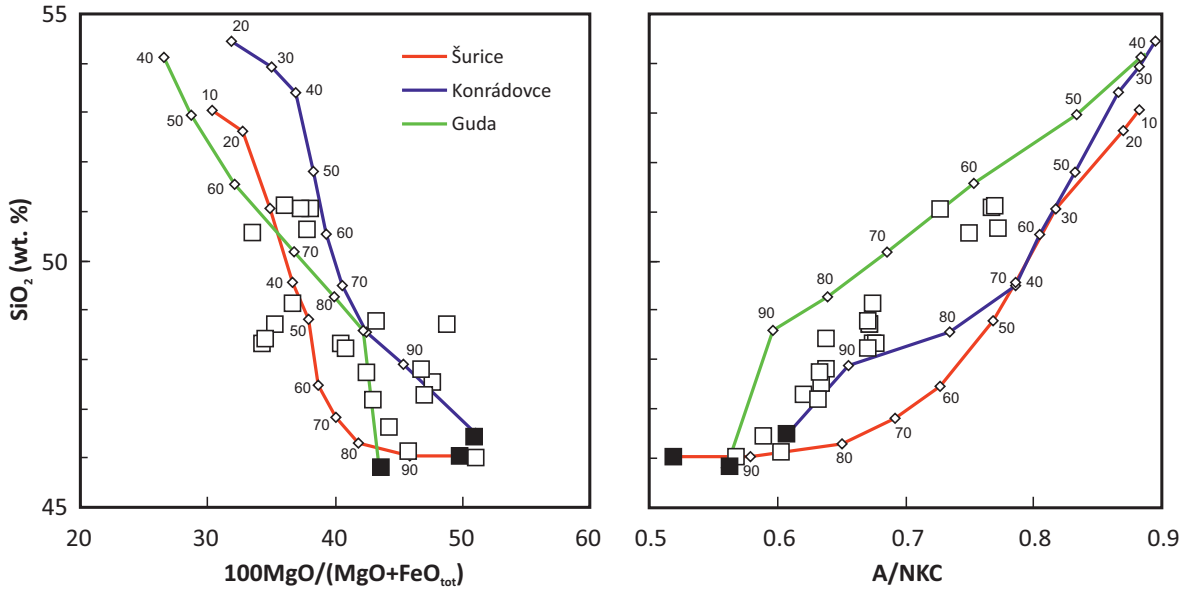

Fig. 16. Fractionation curves of Šurice, Konrádovce and Guda basalts along cooling trajectories depicted in Fig. 15, projected through SiO_2 contents, Mg# numbers, and aluminium saturation index A/NKC = Al_2O_3/Na_2O + K_2O + CaO (molar proportions). Squares are projection points of SSB basalts. Solid squares denote starting basalt compositions employed for the calculation of fractionation models. Diamonds with numbers express the percentages of melt volume fractions remaining after crystallization of solid phases.

that the green clinopyroxenes are products of metasomatic events in the uppermost mantle rather than magma mixing and fractionation. Dobosi & Jenner (1999) and Dobosi et al. (2003) proposed that clinopyroxene megacrysts and associated clinopyroxenite xenoliths may have common origin in mafic cumulates crystallized at Moho depths, although they admitted the green clinopyroxenes to be out of equilibrium with any type of mafic magma. Based on trace elements, Jankovics et al. (2016) suggested metamorphic origin for green clinopyroxene xenocrysts from Bakony–Balaton Highlands incorporated into basaltic magma from lower crustal mafic granulite wall-rocks, and magmatic origin for only few of other clinopyroxenes, representing fragments of pyroxenite cumulates.

The chemical and genetic diversity of homogeneous clinopyroxene megacrysts and oscillatory zoned phenocrysts is manifestated by different substitution vectors (Fig. 9). The following lines of evidence indicate crystallization of unzoned olive-green clinopyroxene megacrysts from evolved Mg-poor silicate melts: (1) alkalic affinity (Fig. 10); (2) crystallization *P–T* conditions plotting between the mantle cluster arranged along 1000 ± 70 °C isotherm (Huraiová & Konečný 1994; Šefara et al. 1995) and the phenocryst cluster between 1100 and 1250 °C (Fig. 13); (3) overlap of *P–T* data obtained in this work with the stability field of pargasitic amphibole located below 1100 °C and 2.9 GPa (Green 2015); (4) apatite–ulvöspinel–carbonate inclusions (Fig. 4F), representing probably a carbonate–phosphate component in hypothetical melt parent; (5) close spatial relationship with apatite megacrysts and pseudomorphs after disintegrated amphibole (Fig. 4). Hence, the simple cumulate model (Dobosi & Jenner 1999; Dobosi et al. 2003) is inadequate for explaining the origin of olive-green clinopyroxene megacrysts. The lower crustal metamorphogenic origin (Jankovics et al. 2016) is applicable to green-cored phenocrysts with Ti# <10, plotting outside the megacrystic trend (Fig. 9).

The assemblage of olive-green clinopyroxene, apatite, spinel, and possibly amphibole megacrysts could be linked with immiscible carbonatite–phosphate–silicate melts percolating in the mantle wedge. Direct evidence for such metasomatic melts was provided by silicate glass pockets in wehrlite xenoliths from Cerová Uplands, where micro-computer tomographic (μ-CT) images revealed up to 5.8 vol. % interstitial glass and up to 3.0 vol. % vesicles originally filled with high-density CO_2 gas in most intensely metasomatised xenoliths (Patkó et al. 2020a). The metasomatic silicate melt component reconstructed from polyphase inlusions in neoformed clinopyroxene corresponded to basaltic andesite and trachyandesite, which evolved to trachyandesite, trachyte and dacite after crystallization of clinopyroxene, amphibole and spinel (Liptai et al. 2021). Carbonatite–melilitite–phosphate melt phases have been described in plagioclase megacrysts and syenite xenoliths in the Hajnáčka diatreme (Hurai et al. 2022). The metasomatic effect of carbonatite–silicate melt on skarnoid xenoliths has been documented from the Čamovce–Belinský vrch lava flow (Reato et al. 2022).

Structure of the lithosphere

Several zones in the lithosphere can be defined by single-pyroxene thermobarometric data (Fig. 13): (1) the continental crust with syenite and hornblendite laccoliths and dykes

representing late-stage derivatives from alkali basalts (<26 km); (2) the Moho discontinuity separating the granulitic lower crust from the lithospheric mantle (26–30 km); (3) the strongly metasomatised mantle (30–45 km) with stagnant basaltic reservoirs producing hornblendite and clinopyroxenite cumulates; (4) the zone of incipient clinopyroxene accumulation from basaltic magma (45–70 km); (5) the partial melting zone (lithosphere–asthenosphere boundary – LAB), where basalts and basanites are generated by the partial melting of fertile peridotite (>70–73 km, >1350 °C). Despite poorer accuracy, ± 0.31 GPa, the single-clinopyroxene thermobarometer reliably identified the zone of basaltic magma underplating and fractionation along the Moho boundary in the depths of 26–30 km, consistently with geophysical data. Lower density, late-stage alkali basalt fractionation derivatives may have propagated up to depths of 24 km beneath the Hodejov maar.

Apart from studies devoted to cumulate xenoliths and megacrysts as cited above, the proposed structural model of the lithospheric mantle is well supported by geophysical data (Tašárová et al. 2009; Bielik et al. 2010; Janik et al. 2011; Horváth et al. 2015; Klébesz et al. 2015) and findings of spinel peridotite xenoliths firstly described in Eresztvény, Magyarbánya (Embey-Isztin 1978), Mašková, Ratka (Hovorka & Fejdi 1980) and in numerous other localities throughout the Cerová Upland (e.g., Szabó & Taylor 1994; Konečný P. et al. 1995; Kovács et al. 2004; Liptai et al. 2019; Patkó et al. 2020a, b).

Conclusions

- Tertiary intra-plate basalts in the South-Slovakian Basin ejected clinopyroxene megacrysts, composite clinopyroxene crystals with homogeneous olive-green cores overgrown by oscillatory zoned rims, and fragments of clinopyroxene-rich igneous cumulates.
- Discrimination based on Ca, Na, Ti and Cr concentrations defined magmatic clinopyroxenes with alkalic, tholeiitic and transitional affinities.
- Single-pyroxene thermobarometric data revealed the incipient clinopyroxene crystallization at 1300–1350 °C and 2.0–2.2 GPa, corresponding to geophysically constrained lithosphere–asthenosphere boundary (LAB) at a depth of ~70–73 km.
- The highest frequency of pressure estimates from mafic cumulates, betwen 0.7 and 1.2 GPa, indicates stagnant basaltic reservoirs beneath the Moho discontinuity (~30 km) up to ~43 km deep. Late clinopyroxene-bearing fractionation products of basalt differentiation (hornblendites) occur as laccoliths or dykes in the lower crust, up to a depth of ~24 km (0.6 GPa).
- Thermodynamic modelling of mineral assemblages from cumulate xenoliths showed similar parental melts for both alkalic and tholeiitic affinities, corresponding to silica-undersaturated, moderately alkalic basanite with the pre-eruptive water content between 1 and 2 wt. %.
- Deep-seated fractionating basalt reservoirs have been less alkalic than majority of surface lavas, the latter showing geochemical fingerprints (Mg depletion inversely correlated with aluminium saturation index) diagnostic of extensive crystal separation on the way to the surface.
- The megacrystic assemblage of Fe-diopside–Al-augite, Mg-calcite, apatite, ulvöspinel, and disintegrated amphibole crystallized from evolved, relatively cold (~950–1100 °C), Fe-rich, carbonatite-alkalic silicate melt within the depth interval from 26 to 53 km. The silicate–carbonate–phosphate liquid was probably released from the subducting slab of oceanic crust.

Data availability: The data that support the findings of this study are available as Electronic Supplementary Material.

Acknowledgements: Analytical works have been funded from the ongoing VEGA project 1/0013/22 and numerous projects finished in previous 20 years. Authors are grateful to two anonymous reviewers and Associate Editor (Dr. Kohút) for stimulating and detailed comments, which significantly improved the initial draft.

References

Balogh K., Miháliková A. & Vass D. 1981: Radiometric dating of basalts in southern and central Slovakia. *Západné Karpaty Séria Geológia* 7, 113–126.

Bielik M., Alasonati-Tašárová Z., Vozár J., Zeyen H., Gutterch A., Grad M., Janik T., Wybraniec S., Götze H.J. & Dérerová J. 2010: Gravity and seismic modelling in the Carpathian-Pannonian Region. In: Vozár J. et al. (Eds.): Variscan and Alpine terranes of the Circum-Pannonian region. *Geological Institute SAS*, Bratislava, 202–233.

Bouloton J. & Paquette J.-L. 2014: In situ U–Pb zircon geochronology of Neogene garnet-bearing lavas from Slovakia (Carpatho–Pannonian region, Central Europe). *Lithos* 184–187, 17–26. https://doi.org/10.1016/j.lithos.2013.10.020

Bracco Gartner A.J.J. & McKenzie D. 2020: Estimates of the temperature and melting conditions of the Carpathian–Pannonian upper mantle from volcanism and seismology. *Geochemistry, Geophysics, Geosystems* 21, e2020GC009334. https://doi.org/10.1029/2020GC009334

Csontos L. 1995: Tertiary tectonic evolution of the intra-Carpathian area: a review. *Acta Vulcanologica* 7, 1–13.

Connolly J.A.D. 2005: Computation of phase equilibria by linear programming: A tool for geodynamic modelling and its application to subduction zone decarbonation. *Earth and Planetary Science Letters* 236, 524–541. https://doi.org/10.1016/j.epsl.2005.04.033

Connolly J.A.D. 2009: The geodynamic equation of state: what and how. *Geochemistry, Geophysics, Geosystems* 10, Q10014. https://doi.org/10.1029/2009GC002540

Dank V. & Fülöp J. (Eds.) 1990: Geological Structural Map of Hungary. *MAFI*, Budapest (in Hungarian).

Diener J.F.A., Powell R., White R.W. & Holland T.J.B. 2007: A new thermodynamic model for clino- and orthoamphiboles in the system Na_2O–CaO–FeO–MgO–Al_2O_3–SiO_2–H_2O–O. *Journal of Metamorphic Geology* 25, 631–656. https://doi.org/10.1111/j.1525-1314.2007.00720.x

Dobosi G. 1989: Clinopyroxene zoning patterns in the young alkali basalts of Hungary and their petrogenetic significance. *Contributions to Mineralogy and Petrology* 101, 112–121. https://doi.org/10.1007/BF00387205

Dobosi G. & Fodor R.V. 1992: Magma fractionation, replenishment, and mixing as inferred from green core clinopyroxenes in Pliocene basanite, southern Slovakia. *Lithos* 28, 133–150. https://doi.org/10.1016/0024-4937(92)90028-W

Dobosi G. & Jenner G.A. 1999: Petrologic implications of trace element variation in clinopyroxene megacrysts from the Nógrád volcanic province, north Hungary: a study by laser ablation microprobe-inductively coupled plasma-mass spectrometry. *Lithos* 46, 731–749. https://doi.org/10.1016/S0024-4937(98)00093-0

Dobosi G., Downes H., Embey-Isztin A. & Jenner G.A. 2003: Origin of megacrysts and pyroxenite xenoliths from the Pliocene alkali basalts of the Pannonian Basin (Hungary). *Neues Jahrbuch für Mineralogie, Abhandlungen* 178, 217–237. https://doi.org/10.1127/0077-7757/2003/0178-0217

Droop G.T.R. 1987: A general equation for estimating Fe^{3+} concentrations in ferromagnesian silicates and oxides from microprobe analyses, using stoichiometric criteria. *Mineralogical Magazine* 51, 431–435. https://doi.org/10.1180/minmag.1987.051.361.10

Dzúrik J., Tomana J. & Vass D. 2007: Rapovce – Geothermal Borehole GTL–2. *Geofond*, Bratislava (in Slovak).

Embey-Isztin A. 1978: On the petrology of spinel lherzolite nodules in basaltic rocks from Hungary and Auvergne, France. *Annales Historico-Naturales Musei Nationalis Hungarici* 70, 27–34.

Embey-Isztin A. & Dobosi G. 1995: Mantle source characteristics for Miocene–Pleistocene alkali basalts, Carpathian–Pannonian Region: a review of trace elements and isotopic composition. *Acta Vulcanologica* 7, 155–166.

Embey-Isztin A., Downes H., James D.E., Upton B.G.J., Dobosi G., Ingram G.A., Harmon R.S. & Scharbert H.G. 1993: The petrogenesis of Pliocene alkaline volcanic rocks from the Pannonian Basin, eastern Central Europe. *Journal of Petrology* 34, 317–343. https://doi.org/10.1093/petrology/34.2.317

Fujii T. & Kushiro I. 1977: Density, viscosity and compressibility of basaltic liquid at high pressures. *Carnegie Institute Washington Year Book* 76, 419–424.

Green D.H. 2015: Experimental petrology of peridotites, including effects of water on melting in the Earth's upper mantle. *Physics and Chemistry of Minerals* 42, 95–122. https://doi.org/10.1007/s00269-014-0729-2

Harangi S., Jankovics M.E., Sági T., Kiss B., Lukács R. & Soós I. 2015: Origin and geodynamic relationships of the Late Miocene to Quaternary alkaline basalt volcanism in the Pannonian Basin, eastern-central Europe. *International Journal of Earth Sciences* 104, 2007–2032. https://doi.org/10.1007/s00531-014-1105-7

Holland T.J.B., Green E.C.R. & Powell R. 2018: Melting of peridotites through to granites: A simple thermodynamic model in the system KNCFMASHTOCr. *Journal of Petrology* 59, 881–900. https://doi.org/10.1093/petrology/egy048

Horváth F., Musitz B., Balázs A., Végh A., Uhrin A., Nádor A., Koroknai B., Pap N., Tóth T. & Wórum G. 2015: Evolution of the Pannonian Basin and its geothermal resources. *Geothermics* 53, 328–352. https://doi.org/10.1016/j.geothermics.2014.07.009

Hovorka D. & Fejdi P. 1980: Spinel peridotite xenoliths in the West Carpathian late Cenozoic alkali basalts and their tectonic significance. *Bulletin Volcanologie* 43, 95–106. https://doi.org/10.1007/BF02597614

Hovorka D. & Lukáčik E. 1972: Xenoliths in andesites of the Massifs Karanč, Šiator (Southern Slovakia) and their geologic interpretation. *Geologický Zborník Geologica Carpathica* 23, 297–303.

Hurai V., Simon K., Wiechert U., Hoefs J., Konečný P., Huraiová M., Pironon J. & Lipka J. 1998: Immiscible separation of metalliferous Fe/Ti-oxide melts from fractionating alkali basalt: P–T–fO_2 conditions and two-liquid elemental partitioning. *Contributions to Mineralogy and Petrology* 133, 12–29. https://doi.org/10.1007/s004100050433

Hurai V., Huraiová M., Konečný P. & Thomas R. 2007: Mineral-melt-fluid composition of carbonate-bearing cumulate xenoliths in Tertiary alkali basalts of southern Slovakia. *Mineralogical Magazine* 71, 63–79. https://doi.org/10.1180/minmag.2007.071.1.63

Hurai V., Paquette J.-L., Huraiová M. & Konečný P. 2010: U–Th–Pb geochronology of zircon and monazite from syenite and pincinite xenoliths in Pliocene alkali basalts of intra-Carpathian back-arc basin. *Journal of Volcanology and Geothermal Research* 198, 275–287. https://doi.org/10.1016/j.jvolgeores.2010.09.012

Hurai V., Danišík M., Huraiová M., Paquette J.-L. & Ádám A. 2013: Combined U/Pb and (U–Th)/He geochronometry of basalt maars in Western Carpathians: implications for age of intraplate volcanism and origin of zircon metasomatism. *Contributions to Mineralogy and Petrology* 166, 1235–1251. https://doi.org/10.1007/s00410-013-0922-1

Hurai V., Huraiová M. & Konečný P. 2021: REE minerals as geochemical proxies of late-Tertiary alkalic silicate±carbonatite intrusions beneath Carpahian back-arc basin. *Minerals* 11, 369. https://doi.org/10.3390/min11040369

Hurai V., Huraiová M., Habler G., Horschinegg M., Milovský R., Milovská S., Hain M. & Abart R. 2022: Carbonatite–melilitite-phosphate immiscible melts from the aragonite stability field entrained from the mantle by a Pliocene basalt. *Mineralogy and Petrology* (in press). https://doi.org/10.1007/s00710-022-00783-1

Huraiová M. & Konečný P. 1994: Pressure–temperature conditions and oxidation state of the upper mantle in southern Slovakia. *Acta Geologica Hungarica* 37, 29–39.

Huraiová M., Konečný P., Konečný V., Simon K. & Hurai V. 1996: Mafic and salic igneous xenoliths in Late Tertiary alkaline basalts: Fluid inclusion and mineralogical evidence for a deep-crustal magmatic reservoir in the Western Carpathians. *European Journal of Mineralogy* 8, 901–916. https://doi.org/10.1127/ejm/8/5/0901

Huraiová M., Konečný P., Holický I., Milovská S., Nemec O. & Hurai V. 2017: Geochemistry, mineralogy, and zircon U–Pb–Hf isotopes of peraluminous A-type granite xenoliths in Pliocene–Pleistocene basalts from northern Pannonian Basin (Slovakia). *Contributions to Mineralogy and Petrology* 172, 59. https://doi.org/10.1007/s00410-017-1379-4

Janik T., Grad M., Guterch A., Vozár J., Bielik M., Vozárová A., Hegedűs E., Kovács C.A., Kovács I., Keller G.R. & CELEBRATION 2000 Working Group 2011: Crustal structure of the Western Carpathians and Pannonian Basin: Seismic models from CELEBRATION 2000 data and geological implications. *Journal of Geodynamics* 52, 97–113. https://doi.org/10.1016/j.jog.2010.12.002

Jankovics M.E., Taracsák Z., Dobosi G., Embey-Isztin A., Batki A., Harangi Sz. & Hauzenberger C.A. 2016: Clinopyroxene with diverse origins in alkaline basalts from the western Pannonian Basin: Implications from trace element characteristics. *Lithos* 262, 120–134. https://doi.org/10.1016/j.lithos.2016.06.030

Jennings E.S. & Holland T.J.B. 2015: A simple thermodynamic model for melting of peridotite in the system NCFMASOCr. *Journal of Petrology* 56, 869–892. https://doi.org/10.1093/petrology/egv020

Kázmér M. & Kovács S. 1985: Permian–Paleogene paleogeography along the eastern part of the Insubric–Periadriatic lineament system: evidence for continental escape of the Bakony–Drauzug Unit. *Acta Geologica Hungarica* 28, 71–84.

Klébesz R., Gráczer Z., Szanyi Gy., Liptai N., Kovács I., Patkó L., Pintér Zs., Falus Gy., Wesztergom V. & Szabó Cs. 2015: Constraints on the thickness and seismic properties of the lithosphere in an extensional setting (Nógrád&Gömör Volcanic Field, Northern Pannonian Basin). *Acta Geodetica et Geophysica* 50, 133–149. https://doi.org/10.1007/s40328-014-0094-0

Konečný P. 2005: Vývoj vrchného plášťa a jeho interakcia so spodnou kôrou na základe zhodnotenia a analýzy xenolitov v oblasti južného Slovenska. Final report 86509-05, *Geofond*, Bratislava.

Konečný P., Konečný V., Lexa J. & Huraiová M. 1995: Mantle xenoliths in alkali basalts of southern Slovakia. *Acta Vulcanologica* 7, 241–247.

Konečný V., Balogh K., Orlický O., Lexa J. & Vass D. 1995: Evolution of the Neogene–Quaternary alkali basalt volcanism in central and southern Slovakia (West Carpathians). *Proceedings of the XI. Congress of Carpatho-Balkan Geological Association*, Athens, 533–538.

Konečný V., Lexa J. & Balogh K. 1999: Neogene–Quaternary alkali basalt volcanism in Central and Southern Slovakia (Western Carpathians). *Geolines* 9, 67–75.

Konečný V., Kováč M., Lexa J. & Šefara J. 2002: Neogene evolution of the Carpatho-Pannonian region: an interplay of subduction and back-arc diapiric uprise in the mantle. *EGU Stephan Mueller Special Publication Series* 1, 105–123. https://doi.org/10.5194/smsps-1-105-2002

Konečný V., Lexa J., Konečný P., Balogh K., Elečko M., Hurai V., Huraiová M., Pristaš J., Sabol M. & Vass D. 2004: Guidebook to the Southern Slovakia Alkali Basalt Volcanic Field. *D. Štúr Geological Institute*, Bratislava, 1–143.

Kovács I., Zajacz Z. & Szabó Cs. 2004: Type-II xenoliths and related metasomatism from the Nógrád–Gömör Volcanic Field, Carpathian–Pannonian region (northern Hungary–southern Slovakia). *Tectonophysics* 393, 139–161. https://doi.org/10.1016/j.tecto.2004.07.032

Kovács I., Patkó L., Liptai N., Lange T.P., Taracsák Z., Cloething S.A.P.L., Török K., Király E., Karátson D., Biró T., Kiss J., Pálos Zs., Aradi L.E., Falus Gy., Hidas K., Berkesi M., Koptev A., Novák A., Wesztergom V., Fancsik T. & Szabó Cs. 2020: The role of water and compression in the genesis of alkaline basalts: Inferences from the Carpathian–Pannonian region. *Lithos* 354–355, 105323. https://doi.org/10.1016/j.lithos.2019.105323

Le Maitre R.W., Streckeisen A., Zanettin B., Le Bas M.J., Bonin B., Bateman P., Bellieni G., Dudek A., Efremova S., Keller J., Lameyre J., Sabine P.A., Schmid R., Sorensen H. & Wooley A.R. 2002: Igneous rocks: a classification and glossary of terms. 2nd Edition. *Cambridge University Press*, Cambridge, 1–236. https://doi.org/10.1017/CBO9780511535581

Leterrier J., Maury R.C., Thonon P., Girard D. & Marchal M. 1982: Clinopyroxene composition as a method of identification of the magmatic affinities of paleo-volcanic series. *Earth and Planetary Science Letters* 59, 139–154. https://doi.org/10.1016/0012-821X(82)90122-4

Lexa J., Seghedi I., Németh K., Szakács A., Konečný V., Pécskay Z, Fülöp A. & Kovacs M. 2010: Neogene–Quaternary volcanic forms in the Carpathian–Pannonian region: a review. *Central European Journal of Geosciences* 2, 207–270. https://doi.org/10.2478/v10085-010-0024-5

Liptai N., Hidas K., Tommasi A., Patkó L., Kovács I.J., Griffon W.L., O´Reilly S.Y., Pearson N.J. & Szabó Cs. 2019: Lateral and vertical heterogeneity in the lithospheric mantle at the northern margin of the Pannonian basin reconstructed from peridotite xenolith microstructures. *Journal of Geophysical Research: Solid Earth* 124, 6315–6336. https://doi.org/10.1029/2018JB016582

Liptai N., Berkesi M., Patkó L., Bodnar R.J., O'Reilly S.Y., Griffin W.L. & Szabó Cs. 2021: Characterization of the metasomatizing agent in the upper mantle beneath the northern Pannonian Basin based on Raman imaging, FIB-SEM, and LA-ICP-MS analyses of silicate melt inclusions in spinel peridotite. *American Mineralogist* 106, 685–700. https://doi.org/10.2138/am-2021-7292

Macdonald G.A. & Katsura T. 1964: Chemical composition of Hawaiian lavas. *Journal of Petrology* 5, 82–133. https://doi.org/10.1093/petrology/5.1.82

Merlet C. 1992: Accurate description of surface ionization in electron probe microanalysis: an improved formulation. *X-Ray Spectrometry* 21, 229–238. https://doi.org/10.1002/xrs.1300210507

Morimoto N., Fabries J., Ferguson A.K., Ginzburg I.V., Ross M., Seifert F.A., Zussman J., Aoki K. & Gottardi G. 1988: Nomenclature of pyroxenes. *American Mineralogist* 73, 1123–1133.

Nemcok M., Pospisil L., Lexa J. & Donelick R.A. 1998: Tertiary subduction and slab break-off model of the Carpathian–Pannonian region. *Tectonophysics* 295, 307–340. https://doi.org/10.1016/S0040-1951(98)00092-4

Nimis P. & Taylor W.R. 2000: Single pyroxene thermobarometry for garnet peridotites. Part I. Calibration and testing of a Cr-in-Cpx barometer and an enstatite-in-Cpx thermometer. *Contributions to Mineralogy and Petrology* 139, 541–554. https://doi.org/10.1007/s004100000156

Paquette J.-L., Huraiová M., Nemec O., Gannoun A., Šarinová K. & Hurai V. 2019: Origin and provenance of 2 Ma–2 Ga zircons ejected by phreatomagmatic eruptions of Pliocene basalts in southern Slovakia. *International Journal of Earth Sciences* 108, 2607–2623. https://doi.org/10.1007/s00531-019-01779-7

Patkó L., Liptai N., Aradi L.E., Klébesz R., Sendula E., Bodnar R.J., Kovács I.J., Hidas K., Cesare B., Novák A., Trásy B. & Szabó Cs. 2020a: Metasomatism-induced wehrlite formation in the upper mantle beneath the Nógrád–Gömör Volcanic Field (Northern Pannonian Basin): evidence from xenoliths. *Geoscience Frontiers* 11, 943–964. https://doi.org/10.1016/j.gsf.2019.09.012

Patkó L., Créon L., Kovács Z., Liptai N., Rosenberg E. & Szabó Cs. 2020b: Three-dimensional distribution of glass and vesicles in metasomatized xenoliths: A micro-CT case study from Nógrád-Gömör Volcanic Field (Northern Pannonian Basin). *Geologica Carpathica* 71, 418–423. https://doi.org/10.31577/GeolCarp.71.5.3

Pécskay Z., Lexa J., Szakács A., Seghedi I., Balogh K., Konečný V., Zelenka T., Kovács M., Póka T., Fülöp A., Márton E., Panaiotu C. & Cvetković V. 2006: Geochronology of Neogene magmatism in the Carpathian arc and intra-Carpathian area. *Geologica Carpathica* 57, 511–530.

Planderová E. 1986: Biostratigraphic evaluation of sediments of the Poltár Formation. *Geologické Práce Správy* 84, 113–118 (in Slovak).

Plašienka D., Grecula P., Putiš M., Kováč M. & Hovorka D. 1997: Evolution and structure of the Western Carpathians: An overview. In: Grecula P., Hovorka D. & Putiš M. (Eds.): Geological Evolution of the Western Carpathians. *Mineralia Slovaca Monograph*, *Geocomplex*, Bratislava, 1–24.

Putirka K.D. 2008: Thermometers and barometers for volcanic systems. *Reviews in Mineralogy and Geochemistry* 69, 61–120. https://doi.org/10.2138/rmg.2008.69.3

Putirka K., Johnson M., Kinzler R., Longhi J. & Walker D. 1996: Thermobarometry of mafic igneous rocks based on clinopyroxene-liquid equilibria, 0–30 kbar. *Contributions to Mineralogy and Petrology* 123, 92–108. https://doi.org/10.1007/s004100050145

Putirka K., Ryerson F.J. & Mikaelian H. 2003: New igneous thermobarometers for mafic and evolved lava compositions, based on clinopyroxene + liquid equilibria. *American Mineralogist* 88, 1542–1554. https://doi.org/10.2138/am-2003-1017

Reato L., Huraiová M., Konečný P., Marko F. & Hurai V. 2022: Formation of esseneite and kushiroite in tschermakite-bearing calc-silicate xenoliths ejected in alkali basalt. *Minerals* 12, 156. https://doi.org/10.3390/min12020156

Royden L.H., Horváth F., Nagymarosy A. & Stegena F. 1983: Evolution of the Pannonian Basin system. 2. Subsidence and thermal history. *Tectonics* 2, 91–137. https://doi.org/10.1029/TC002i001p00091

Seghedi I., Downes H., Vaselli O., Szakács A., Balogh K. & Pécskay Z. 2004: Post-collisional Tertiary–Quaternary mafic alkalic magmatism in the Carpathian-Pannonian region: A review. *Tectonophysics* 393, 43–62. https://doi.org/10.1016/j.tecto.2004.07.051

Seghedi I., Maţenco L., Downes H., Mason P.R.D., Szakács A. & Pécskay Z. 2011: Tectonic significance of changes in post-subduction Pliocene–Quaternary magmatism in the south east part of the Carpathian–Pannonian Region. *Tectonophysics* 502, 146–157. https://doi.org/10.1016/j.tecto.2009.12.003

Snopková P. & Bajaník Š. 1979: Evidence of Devonian (Givetian–Frasnian) in borehole FV-1 Blhovce. *Geologické Práce Správy* 72, 7–17 (in Slovak).

Szabó Cs. & Bodnar R.J. 1998: Fluid-inclusion evidence for an upper-mantle origin for green clinopyroxenes in late Cenozoic basanites from the Nógrád–Gömör Volcanic Field, northern Hungary/southern Slovakia. *International Geology Review* 40, 765–773. https://doi.org/10.1080/00206819809465237

Szabó Cs. & Taylor L.A. 1994: Mantle petrology and geochemistry beneath Nógrád–Gömör Volcanic Field, Carpathian–Pannonian region. *International Geology Review* 36, 328–358. https://doi.org/10.1080/00206819409465465

Šefara J., Bielik M., Konečný P., Bezák V. & Hurai V. 1995: The latest stage of development of the lithosphere and its interaction with the asthenosphere (Western Carpathians). *Geologica Carpathica* 47, 339–347.

Tašárová A., Afonso J.C., Bielik M., Götze H.-J. & Hók J. 2009: The lithospheric structure of the Western Carpathian-Pannonian Basin region based on the CELEBRATION 2000 seismic experiment and gravity modeling. *Tectonophysics* 475, 454–469. https://doi.org/10.1016/j.tecto.2009.06.003

Vass D. & Kraus I. 1985: Two basalts of different age in southern Slovakia and their relation to the Poltár Formation. *Mineralia Slovaca* 17, 435–440 (in Slovak).

Vass D., Began A., Gross P., Kahan Š, Köhler E., Lexa J. & Nemčok J. 1988a: Regional Geological Division of the Western Carpathians and the Northern Promontory of the Pannonian Basin in the Territory of the Czechoslovak Republic. Map 1:500,000. *D. Štúr Geological Institute*, Bratislava (in Slovak).

Vass D., Bajaník Š., Husák Ľ., Kantorová V., Lehotayová R., Marková M., Ondrejičková A., Snopková P. & Vozárová A. 1988b: Structural borehole FV–1 Blhovce (2100 m). *Regionálna Geológia Západných Karpát* 23, 7–86 (in Slovak).

Vass D., Elečko M., Konečný V., Krippel M., Kubeš P., Lexa J., Pristaš J., Zakovič M., Vozár J., Vozárová A., Bodnár J., Husák Ľ., Filo M., Lacika J. & Linkeš V. 2007: Geology of the Lučenská Kotlina Basin and Cerová Vrchovina Mts. *D. Štúr Geological Institute*, Bratislava, 1–284 (in Slovak).

Wilson M. & Downes H. 1991: Tertiary–Quaternary extension-related alkaline magmatism in western and central Europe. *Journal of Petrology* 32, 811–849. https://doi.org/10.1093/petrology/32.4.811

Zajacz Z., Kovács I., Szabó C., Halter W. & Pettke T. 2007: Evolution of mafic alkaline melts crystallized in the uppermost lithospheric mantle: a melt inclusion study of olivine-clinopyroxenite xenoliths, northern Hungary. *Journal of Petrology* 48, 853–883. https://doi.org/10.1093/petrology/egm004

Electronic supplementary material is available online:
Supplementary Tables S1–S3 at http://geologicacarpathica.com/data/files/supplements/GC-74-4-Hurai_TablesS1-S3.xlsx